Increased association between Epstein-Barr virus EBNA2 from type 2 strains and the transcriptional repressor BS69 restricts B cell growth

Rajesh Ponnusamy[1], Ritika Khatri[1], Paulo B. Correia[2], Erika Mancini[1], Paul J. Farrell[2] and Michelle J. West[1*]

1. School of Life Sciences, University of Sussex, Falmer, Brighton, BN1 9QG, UK.

2. Section of Virology, Imperial College London, Norfolk Place, London W2 1PG, UK.

* To whom correspondence should be addressed. Tel: +44 (0)1273 678404; Fax: +44 (0)1273 877586; Email: m.j.west@sussex.ac.uk

Abstract

Natural variation separates Epstein-Barr virus (EBV) into type 1 and type 2 strains. Type 2 EBV is less transforming *in vitro* due to sequence differences in the EBV transcription factor EBNA2. This correlates with reduced activation of the EBV oncogene LMP1 and some cell genes. Transcriptional activation by type 1 EBNA2 can be suppressed through the binding of two PXLXP motifs in its transactivation domain (TAD) to the dimeric coiled-coil MYND domain (CC-MYND) of the BS69 repressor protein (ZMYND11). We identified a third conserved PXLXP motif in type 2 EBNA2. We found that type 2 EBNA2 peptides containing this motif bound $BS69_{CC\text{-}MYND}$ efficiently and that the type 2 $EBNA2_{TAD}$ bound an additional $BS69_{CC\text{-}MYND}$ molecule. Full-length type 2 EBNA2 also bound BS69 more efficiently in pull-down assays. Molecular weight analysis and low-resolution structures obtained using small-angle X-ray scattering showed that three $BS69_{CC\text{-}MYND}$ dimers bound two molecules of type 2 $EBNA2_{TAD}$, in line with the dimeric state of full-length EBNA2 *in vivo*. Importantly, mutation of the third BS69 binding motif in type 2 EBNA2 improved B-cell growth maintenance. Our data indicate that increased association with BS69 restricts growth promotion by EBNA2 and may contribute to reduced B-cell transformation by type 2 EBV.

Author summary

Epstein-Barr virus (EBV) drives the development of many human cancers worldwide including specific types of lymphoma and carcinoma. EBV infects B lymphocytes and immortalises them, thus contributing to lymphoma development. The virus promotes B lymphocyte growth and survival by altering the level at which hundreds of genes are expressed. The EBV protein EBNA2 is known to activate many growth-promoting genes. Natural variation in the sequence of EBNA2 defines the two main EBV strains: type 1 and type 2. Type 2 strains immortalise B lymphocytes less efficiency and activate some growth genes poorly, although the mechanism of this difference is unclear. We now show that sequence variation in type 2 EBNA2 creates a third site of interaction for the repressor protein (BS69, ZMYND11). We have characterised the complex formed between type 2 EBNA2 and BS69 and show that three dimers of BS69 form a bridged complex with two molecules of type 2 EBNA2. We demonstrate that mutation of the additional BS69 interaction site in type 2 EBNA2 improves its growth-promoting function. Our results therefore provide a molecular explanation for the different B lymphocyte growth promoting activities of type 1 and type 2 EBV. This aids our understanding of immortalisation by EBV.

54 **Introduction**

55 Epstein-Barr virus (EBV) is a ubiquitous γ-herpesvirus that immortalises human B
56 lymphocytes to establish a lifelong persistent infection that is usually harmless. Delayed
57 primary EBV infection can however give rise to infectious mononucleosis. EBV is also
58 associated with the development of malignancies that include Burkitt's (BL), Hodgkin's,
59 diffuse large B cell and post-transplant lymphoma and nasopharyngeal or gastric carcinoma.
60 EBV expresses nine latent proteins in *in vitro* infected lymphoblastoid cell lines (LCLs),
61 including 6 Epstein-Barr nuclear antigens (EBNA1, 2, 3A, 3B, 3C and leader protein) and 3
62 latent membrane proteins (LMP1, 2A, 2B). The EBNA2 transcription factor is one of five of
63 these latent genes essential for B cell transformation (1). EBNA2 functions as the master
64 regulator of EBV latent gene transcription and activates numerous cell genes that control B cell
65 growth and survival (2). It cannot however bind to DNA directly and hijacks cell DNA binding
66 proteins e.g. RBPJ (RBPJκ, CBF1) and EBF1 to target viral and cell gene regulatory elements
67 (2, 3). Although EBNA2 binding sites are close to gene promoters in the viral genome, in the
68 B cell genome they are mostly found at enhancer elements and EBNA2 has been shown to
69 promote enhancer-promoter interactions (4-6). EBNA2 activates transcription through
70 interactions between its acidic transactivation domain (TAD) and histone acetyl transferases,
71 ATP-dependent remodellers and components of the preinitiation complex (7-13).

72

73 EBV genome sequences worldwide separate into two main strains (type 1 and type 2) based on
74 differences in the EBNA2 and EBNA3A, 3B and 3C genes (14-18). Type 2 strains are less
75 efficient at immortalising resting B cells *in vitro* than type 1 strains (19). This phenotype is
76 determined by sequence variation in EBNA2 since complementation of an EBNA2 defective
77 virus with type 1 EBNA2 but not type 2 EBNA2 supports efficient primary B cell

immortalisation (1). Consistent with its reduced primary B cell transforming function, type 2 EBNA2 cannot complement loss of type 1 EBNA2 function to maintain the growth of lymphoblastoid cell lines (20). Amino acids responsible for the differences in B cell growth maintenance between type 1 and type 2 EBNA2 were mapped to the C-terminal region of EBNA2 (20). Surprisingly, a single amino acid (aspartate 442 of type 1 EBNA2) in the TAD appears to be a key determinant of B cell growth maintenance by type 1 EBNA2. Replacing the serine that occurs at the equivalent position in type 2 EBNA2 (amino acid 409 of type 2 EBNA2) with aspartate (mutant S442D) confers efficient growth maintenance function (21). Type 2 EBNA2 has reduced ability to activate expression of the EBV oncogene LMP1 and a small number of cellular genes e.g. CXCR7 (22). These differences in gene activation could underlie the reduced B cell growth maintenance and transforming function of type 2 EBNA2, although the mechanism involved and the role played by the single aspartate residue is unclear. Part of the mechanism may involve (or result in) reduced binding of type 2 EBNA2 to the LMP1 promoter and cell gene regulatory elements (21). EBNA2 binding sites at genes activated less efficiently by type 2 EBNA2 are enriched for composite binding motifs for ETS and IRF transcription factors (ETS and IRF composite element; EICE), implicating ETS/IRF family members in the gene specificity of the observed effects (21).

Despite a clear deficiency in the immortalising and B cell growth maintenance properties of type 2 EBNA2 *in vitro*, no specific differences in disease association have been reported to date for type 1 and type 2 EBV. Interestingly, although the outgrowth of immortalised cells is less efficient and much slower in primary B cell cultures infected with type 2 EBV (19, 20), the LCLs that are eventually established from type 2 viruses proliferate at similar rates to type 1 LCLs. Type 1 and 2 LCLs also show equivalent expression of LMP1 and CXCR7 (20). Over extended periods of time, it is therefore possible to select for immortalised cells infected with

103 type 2 EBV that have the required levels of expression of these genes to support their long term
104 proliferation. *In vivo* other factors may create an environment that helps support B cell
105 immortalisation by type 2 EBV.

106

107 New research also suggests that type 2 EBV may use alternative approaches to persist *in vivo*.
108 Type 2 EBV has the unique capacity to infect T cells in culture and is detected in T cells from
109 healthy infants from Kenya, indicating that T cell infection may form part of a natural type 2
110 EBV infection (23, 24). Recent work also showed that a type 2 EBV strain was able to infect
111 both B cells and T cells in humanised mice (25). Mice infected with type 2 EBV developed
112 tumours that resembled the diffuse large B-cell lymphomas that also developed in mice infected
113 with type 1 EBV, confirming the tumorigenic potential of a persistent type 2 EBV infection,
114 once established (25).

115

116 BS69 (ZMYND11) is a multi-domain chromatin-associated repressor protein that suppresses
117 transcription elongation, regulates pre-mRNA processing and has tumour suppressor function
118 (26, 27). The BS69 gene undergoes chromosomal translocation in minimally differentiated
119 myeloid leukaemia leading to the expression of a BS69-MBTD1 fusion protein (28). BS69
120 contains three histone reader domains in its N-terminal region; a plant homeodomain, a
121 bromodomain and a PWWP domain. The tandemly-arranged bromodomain and PWWP
122 domain bind to histone H3 or the variant histone H3.3 when trimethylated on lysine K36 (27,
123 29). BS69 also contains a coiled-coil (CC) dimerisation domain adjacent to a MYND domain
124 in its C terminus. BS69 binds to a number of chromatin modifying enzymes (BRG1, HDAC1,
125 EZH2) and transcription factors (adenovirus E1a, c-Myb, ETS2, E2F6, and the Myc-associated

126 MGA protein) and inhibits transcription factor activation function (30-34). The BS69 MYND
127 domain binds to E1a and MGA through a PXLXP motif (34).

128

129 BS69 has also been shown to interact with the TAD of type 1 EBNA2 through two PXLXP
130 motifs and to restrict EBNA2 transcriptional activation function (34, 35). The structure of the
131 dimeric CC-MYND domain of BS69 bound to two peptides encompassing sequences from one
132 of the EBNA2 PXLXP motifs (motif 1) has been solved (35). Based on this three-dimensional
133 structure, a BS69 dimer was predicted to interact with the two adjacent PXLXP motifs in type
134 1 EBNA2. Interestingly the amino acid implicated in the type-specific differences in growth
135 maintenance observed for type 1 and type 2 EBNA2 (amino acid 442 in type 1 EBNA2) (21)
136 lies immediately adjacent to the second BS69 binding motif.

137

138 We set out to determine whether sequence differences between type 1 and type 2 EBNA2 affect
139 BS69 binding. We hypothesised that type 2 EBNA2 would show increased binding to BS69
140 and that this would impair its gene activation and growth maintenance function. We initially
141 examined the impact of type-specific differences in EBNA2 amino acid 442 on BS69 binding.
142 We also identified a third PXLXP BS69 binding motif in type 2 EBNA2, so we examined
143 whether the presence of this extra motif resulted in the interaction of additional molecules of
144 BS69 with type 2 EBNA2. We found that amino acid 442 did not affect BS69 binding, but
145 influenced the conformation of the TAD, potentially affecting binding of other transcriptional
146 regulators. We also demonstrated that the third PXLXP motif in type 2 EBNA2 was responsible
147 for the binding of an additional BS69 dimer. Importantly, mutation of the third PXLXP BS69
148 binding motif in full length type 2 EBNA2 restored B cell growth maintenance function
149 indicating that increased BS69 binding is responsible for impaired type 2 EBNA2 function.

150

151 **Results**

152 *Sequence differences near type 2 EBNA2 BS69 binding motif 2 do not increase BS69 binding.*

153 Previous studies demonstrated that differences in a single amino acid in the TAD between type
154 1 and type 2 EBNA2 determined the ability of EBNA2 to maintain the growth of an EBV-
155 infected LCL (21). This amino acid (located at position 442 in the EBNA2 sequence from the
156 prototypical type 1 B95-8 strain of EBV) is conserved as aspartate in type 1 strains and as
157 serine (at the corresponding position of 409) in type 2 strains. In type 1 EBNA2, aspartate 442
158 is located immediately adjacent to a previously identified binding motif for the cell
159 transcriptional repressor BS69 (motif 2) that fits the PXLXP consensus ($PILFP_{437-441}$)(34). In
160 the TAD of type 2 EBNA2, the PXLXP motif is conserved ($PFLFP_{404-408}$) and is flanked by
161 serine 409 (Figure 1A).

162

163 We hypothesised that the impaired gene activation and growth maintenance properties of type
164 2 EBNA2 may be the result of increased binding to BS69 as a result of the aspartate to serine
165 amino acid difference adjacent to BS69 binding motif 2. We therefore tested whether a BS69
166 binding motif 2 peptide from type 2 EBNA2 showed enhanced binding to BS69 compared to
167 a motif 2 peptide from type 1 EBNA2. We used isothermal titration calorimetry (ITC) to
168 determine the affinity of peptide binding to the C-terminal region of BS69 (amino acid 480-
169 602) comprising the CC-MYND domain that we expressed and purified from *E.coli* (Figure
170 1B and 1C). In contrast to our hypothesis, we found that the type 2 EBNA2 motif 2 peptide
171 bound to $BS69_{CC-MYND}$ with reduced affinity (K_D=176 μM) compared to the corresponding
172 peptide from type 1 EBNA 2 (K_D=47.7 μM) (Figure 1B and 1C and Supplementary Table S1).
173 The affinity of binding of the type 1 EBNA 2 motif 2 peptide to $BS69_{CC-MYND}$ was very similar
174 to the previously reported K_D of 35 μM (35). The difference in binding between type 1 and

175 type 2 EBNA2 motif 2 peptides could be influenced by both the aspartate to serine change and
176 differences in two other amino acids present in the sequence (Figure 1B and 1C).

177

178 An additional BS69 PXLXP binding motif previously identified in type 1 EBNA2 (motif 1)
179 located N-terminal to motif 2 is also present in type 2 EBNA 2 (Figure 1A). The $BS69_{CC\text{-}MYND}$
180 dimer binds a type 1 EBNA2 polypeptide containing both motif 1 and motif 2 with high affinity
181 and the structure of BS69 dimer could accommodate binding to both motifs simultaneously
182 (35). We therefore tested whether sequence differences in type 2 EBNA2 (including the
183 aspartate to serine change) affected the binding of a region of EBNA2 containing both motif 1
184 and motif 2 to BS69. Type 1 $EBNA2_{381\text{-}445}$ and type 2 $EBNA2_{348\text{-}412}$ were expressed and
185 purified from *E.coli* and their interaction with $BS69_{CC\text{-}MYND}$ examined using ITC. Consistent
186 with previous reports (35) we found that type 1 $EBNA2_{381\text{-}445}$ bound to $BS69_{CC\text{-}MYND}$ with high
187 affinity (K_D=0.95 μM) likely due to the high avidity of interaction with two binding sites
188 (Figure 1D). In the context of this larger region of EBNA2 we found very little difference in
189 the affinity of type 2 EBNA2 binding to $BS69_{CC\text{-}MYND}$ (K_D=1.21 μM) (Figure 1E). In addition
190 to measuring binding affinities, ITC data can also be used to calculate binding stoichiometry
191 (n) which can be visualised as the molar ratio at the mid (inflection) point of the sigmoidal
192 binding curve. We titrated EBNA2 polypeptides into a cell containing $BS69_{CC\text{-}MYND,}$ so the
193 stoichiometry values we obtained indicate the molar ratio at which the EBNA2 polypeptide
194 saturates the available sites in $BS69_{CC\text{-}MYND}$ monomers. Consistent with the presence of two
195 BS69 binding sites in the EBNA2 polypeptides, we obtained n values of 0.42 and 0.33 for type
196 1 and type 2 EBNA2: $BS69_{CC\text{-}MYND}$ binding, respectively (Figure 1D and 1E). These
197 approximate to the expected molar ratio of 0.5 taking into consideration some margin of error
198 in n value determination by ITC, which is heavily influenced by the accuracy of protein
199 concentrations and the proportion of 'active' protein in the sample.

200

201 We conclude that the aspartate 442 to serine amino acid difference between type 1 and type 2
202 EBNA2 does not affect the binding of BS69 to the TAD of type 2 EBNA2 in these assays. Our
203 data also indicate that additional sequence differences in and around BS69 binding motifs 1
204 and 2 in type 2 EBNA2 do not influence the binding of the $BS69_{CC\text{-}MYND}$ dimer to this region
205 of the protein.

206

207 *Type 2 EBNA2 contains a third BS69 binding site*

208 During the course of our study we also identified a third potential BS69 binding site in the type
209 2 EBNA2 TAD (Figure 2A). In type 2 EBNA2, a sequence that is an exact match to the PXLXP
210 BS69 consensus binding motif is present C-terminal to motif 2 ($PTLEP_{414\text{-}418}$). In type 1
211 EBNA2 the corresponding region has an isoleucine in place of the leucine residue ($PSIDP_{447\text{-}}$
212 $_{451}$). To determine whether these regions of EBNA2 also interact with BS69, we performed
213 ITC experiments using type 1 and type 2 EBNA2 peptides (Figure 2B and 2C). We were not
214 able to detect any binding of the type 1 EBNA2 peptide encompassing this region (T1
215 $EBNA2_{445\text{-}455}$) to $BS69_{CC\text{-}MYND}$, underscoring the importance of the central leucine in the
216 PXLXP motif for the BS69 interaction (Figure 2B). In contrast, a peptide from the
217 corresponding region of type 2 EBNA2 (T2 $EBNA2_{412\text{-}422}$) interacted with BS69 with a
218 K_D=219 μM (Figure 2C). The affinity of interaction with this new motif (that we named motif
219 3) is weaker than the interaction we observed for type 1 or type 2 EBNA2 motif 2 (Figure 1).
220 To determine the impact of motif 3 on the interaction of type 2 EBNA2 with $BS69_{CC\text{-}MYND}$ in
221 the presence of the two other BS69 binding motifs, we expressed and purified a larger type 2
222 EBNA2 polypeptide containing motif 1, 2 and 3 (T2 $EBNA2_{348\text{-}422}$) for use in ITC. For
223 comparison, we also analysed the binding of the corresponding larger region of type 1 EBNA2

224 (T1 EBNA2$_{381-455}$). We found that inclusion of the additional C-terminal amino acids had little
225 impact on the affinity of binding of type 1 EBNA2 to BS69$_{CC-MYND}$ or the stoichiometry of
226 binding (compare Figure 2D and Figure 1D) (Supplementary Table S2). In contrast, for type 2
227 EBNA2, we observed a change in the stoichiometry of binding from 0.33 when motif 1 and 2
228 were present (T2 EBNA2$_{348-412)}$ to 0.15 when motif 1, 2 and 3 were present (T2 EBNA2$_{348-422}$)
229 (compare Figure 2E and 1E). This is consistent with the presence of an additional BS69 binding
230 site and indicates the interaction of T2 EBNA2$_{348-422}$ with an additional BS69$_{CC-MYND}$ molecule.
231 Perhaps surprisingly, we did not observe an increase in the affinity of binding of the longer
232 type 2 EBNA2 polypeptide to BS69$_{CC-MYND}$ (compare Figure 2E and 1E). Nonetheless the
233 recruitment of more BS69 to type 2 EBNA2 could be physiologically relevant for the function
234 of type 2 EBNA2 as a transcriptional activator. To confirm that the observed change in binding
235 stoichiometry was due to the presence of motif 3 in the type 2 EBNA2 polypeptide, we analysed
236 the binding of T2 EBNA2$_{348-422}$ with motif 3 mutated from PTLEP to ATAEA (T2 EBNA2$_{348-}$
237 $_{422}$ motif 3 mt). We found that mutation of motif 3 altered the stoichiometry of binding to
238 BS69$_{CC-MYND}$ from 0.15 to 0.30, consistent with the loss of a BS69 binding motif (Figure 2F).
239 This is similar to the value obtained for the type 2 EBNA2 polypeptide containing only motif
240 1 and motif 2 (T2 EBNA2$_{348-412}$)(Figure 1E). We conclude that type 2 EBNA2 contains an
241 additional binding site for BS69 that is not present in type 1 EBNA2.

242

243 *Three BS69 CC-MYND dimers bridge two molecules of type 2 EBNA2*

244 To further examine whether type 2 EBNA2 could form higher-order complexes with the BS69
245 CC-MYND domain that are larger than type 1 EBNA2, we examined the properties of BS69-
246 EBNA2 complexes using size exclusion chromatography (SEC). Consistent with complex
247 formation, when pre-incubated with BS69$_{CC-MYND,}$ both T1 EBNA2$_{381-455}$ and T2 EBNA2$_{348-422}$

248 polypeptides migrated through the size exclusion column faster and eluted at a lower elution
249 volume compared to the migration of each component individually (Figure 3A). In line with
250 the binding of additional $BS69_{CC\text{-}MYND}$ molecules to T2 $EBNA2_{348\text{-}422}$ and the formation of
251 higher molecular weight complexes, we found that type 2 EBNA2 complexes eluted at a lower
252 volume than type 1 EBNA2 complexes (Figure 3A). SDS-PAGE of SEC column fractions
253 confirmed the presence of $BS69_{CC\text{-}MYND}$ and EBNA2 in the higher molecular weight complexes
254 (Figure 3B). Note that both type 1 and type 2 EBNA2 polypeptides migrate anomalously on
255 SDS-PAGE gels and not at their predicted molecular weights (MW) of 7.9 and 8.1 kDa
256 respectively, likely due to their high proline content (Figure 3B). They are however pure and
257 resolve as single species on gel filtration columns (Figure 3A).

258

259 Because migration in SEC is influenced by both size and shape and $BS69_{CC\text{-}MYND}$ has an
260 elongated structure due to the CC domain, we were unable to determine the MW of BS69-
261 EBNA2 complexes accurately using SEC. In order to obtain more accurate MW information
262 that would allow us to determine the number of molecules of $BS69_{CC\text{-}MYND}$ and EBNA2 present
263 in type 1 and type 2 complexes, we used SEC with multi-angle light scattering (SEC-MALS)
264 (Table 1). SEC-MALS gave MWs for T1 $EBNA2_{381\text{-}455}$ and T2 $EBNA2_{348\text{-}422}$ that matched the
265 theoretical MW of their monomeric forms and gave a MW for $BS69_{CC\text{-}MYND}$ consistent with its
266 dimeric state (Table 1). For the T1 $EBNA2_{381\text{-}455}$-$BS69_{CC\text{-}MYND}$ complex, SEC-MALS gave a
267 MW of 62.3 kDa. Given that there are two binding sites for BS69 in the T1 $EBNA2_{381\text{-}455}$
268 polypeptide, this figure most closely matches the MW of a complex containing two type 1
269 EBNA2 polypeptides and two $BS69_{CC\text{-}MYND}$ dimers (theoretical MW of 76.7 kDa) rather than
270 a single type 1 EBNA2 polypeptide with a one dimer of EBNA2 $BS69_{CC\text{-}MYND}$ (theoretical MW
271 of 38.3 kDa) (Table 1). For the $BS69_{CC\text{-}MYND}$-T2 $EBNA2_{348\text{-}422}$ complex, SEC-MALs gave a
272 MW of 135 kDa consistent with the larger complex size observed in SEC (Table 1 and Figure

273 3A). Given the presence of three BS69 binding motifs in type 2 EBNA2, this MW most closely
274 matches that of a complex containing three $BS69_{CC\text{-}MYND}$ dimers and two type 1 EBNA2
275 polypeptides (theoretical MW of 107.5 kDa) (Table 1).

276

277 Because of the discrepancies in the theoretical and experimentally determined MWs for
278 $BS69_{CC\text{-}MYND}$-EBNA2 complexes, we also used small-angle-X-ray scattering (SAXS) to obtain
279 information on the shape and size of these complexes in solution. Initially we used SEC-SAXS
280 to analyse each polypeptide individually. We used a Kratky representation to visualize features
281 of the scattering profiles obtained for T1 $EBNA2_{381\text{-}45,}$ T2 $EBNA2_{348\text{-}422}$ and $BS69_{CC\text{-}MYND}$
282 individually to identify the folding state of the polypeptides in solution. The absence of a bell-
283 shaped curve with a well-defined maximum for both EBNA2 polypeptides indicates that they
284 are natively unfolded in solution (Supplementary Figure S1). The bell-shaped curve obtained
285 for the $BS69_{CC\text{-}MYND}$ dimer indicates that it is folded in solution as expected from the crystal
286 structure (35). Three-dimensional models were created for the individual polypeptides by *ab*
287 *initio* shape determination. For $BS69_{CC\text{-}MYND}$ a solution structure consistent with the coiled-
288 coil dimer structure determined by X-ray crystallography was obtained (35)(Supplementary
289 Figure S2). For the EBNA2 polypeptides, solution structures consistent with flexible unfolded
290 peptide chains were obtained (Supplementary Figure S2). SAXS analysis of $BS69_{CC\text{-}MYND}$ pre-
291 mixed with either type 1 or type 2 EBNA2 polypeptides gave a larger Porod volume (directly
292 related to MW) compared to the individual proteins, consistent with complex formation
293 (Supplementary Table S3). An *ab initio* dummy atom model was generated for the type 1
294 EBNA2-$BS69_{cc\text{-}MYND}$ complex and this fitted well to the experimental SAXS data (χ^2 of 1.4)
295 (Figure 4A). The three-dimensional model generated by *ab initio* shape determination for the
296 type 1 EBNA2-$BS69_{cc\text{-}MYND}$ complex indicated that the complex has a large elongated shape
297 with a volume of 166 nm^3 and a maximum dimension (Dmax) of 138 Å (Figure 4B). This three-

298 dimensional model could accomodate two $BS69_{CC\text{-}MYND}$ dimer structures that were manually
299 docked into the SAXS envelope. The additional space at the bottom of the model was allocated
300 to the model solution structures of two type 1 EBNA2 polypeptides (Figure 4B). This docked
301 structural model for the type 1 EBNA2-$BS69_{CC\text{-}MYND}$ complex was then fitted to the
302 experimental scattering data and gave a reasonable χ^2 value of 2.56. For comparison a structural
303 model where only one $BS69_{CC\text{-}MYND}$ dimer and a single type 1 EBNA2 polypeptide were
304 docked into the SAXS envelope was created but this alternative model gave a worse fit to the
305 experimental data (Supplementary Figure S3). An *ab initio* dummy atom model was then
306 generated for the type 2 EBNA2-$BS69_{CC\text{-}MYND}$ complex and this fitted well to the experimental
307 SAXS data (χ^2 of 1.0) (Figure 4C). The three-dimensional model created by *ab initio* shape
308 determination for the type 2 EBNA2 complex had a larger volume (239 nm^3) and maximum
309 dimension (145 Å) than the type 1 EBNA2 complex model (Figure 4D). The type 2 EBNA2
310 model could accommodate the docking of three $BS69_{CC\text{-}MYND}$ dimer structures along with two
311 type 2 EBNA2 polypeptides and this structural model gave a good fit to the experimental data
312 (χ^2 of 1.44) (Figure 4C and D). In comparison a docked model containing two $BS69_{CC\text{-}MYND}$
313 dimers and a single type 2 EBNA2 polypeptide gave a worse fit to the experimental data
314 (Supplementary Figure S3).

315

316 Taken together our data indicate that BS69 forms higher order complexes with EBNA2 that
317 involve the interaction of each MYND domain of the BS69 dimer with binding sites in two
318 separate EBNA2 molecules. Rather than an *in vitro* artefact, this intermolecular 'bridging'
319 interaction is consistent with the fact that EBNA2 forms dimers *in vivo*. Although the N-
320 terminal regions of EBNA2 that mediate dimerisation (36) are absent in the EBNA2
321 polypeptides we examined in our interaction studies, our data indicate that BS69 may have the
322 capacity to stabilise or enhance dimerisation between two EBNA2 molecules held together

323 through their N-termini. Importantly, using multiple independent techniques, we also
324 demonstrate that type 2 EBNA 2 interacts with an additional $BS69_{CC\text{-}MYND}$ dimer.

325

326 *The serine to aspartate change in type 2 EBNA2 alters its binding characteristics*

327 During the course of our ITC experiments we observed that binding data obtained using the
328 longer EBNA2 polypeptides (T1 $EBNA2_{381\text{-}455}$ and T2 $EBNA2_{348\text{-}422}$) showed some deviation
329 from curves fitted using the single binding event ('one set of sites') model (where binding to
330 multiple sites cannot be detected as separate heat change events) (Figure 2D and 2E). This
331 suggested that the mode of binding of these polypeptides to $BS69_{CC\text{-}MYND}$ could involve more
332 than one distinguishable binding event. To determine whether this was the case, we performed
333 ITC experiments using an increased number of smaller injections of the EBNA2 polypeptide
334 to obtain more data points for curve fitting (Figure 5). For T1 $EBNA2_{381\text{-}455}$ the binding data
335 did not fit well to curves generated using an alternative two binding event ('two sets of sites')
336 model (χ^2/degrees of freedom=0.56) (Figure 5A and Supplementary Table S2). This indicates
337 that the deviation of T1 $EBNA2_{381\text{-}455}$-$BS69_{CC\text{-}MYND}$ binding data from fitted curves at low
338 molar ratios was unlikely to be the result of a separate binding event (Figure 2D and 5A). In
339 contrast, for T2 $EBNA2_{348\text{-}422}$ the binding profiles obtained fitted well to curves generated using
340 the two binding event model (χ^2/degrees of freedom=0.23) (Figure 5B and Supplementary
341 Table S2). This enabled the affinity of the two separate binding events to be determined, which
342 were both in the nanomolar range (K_{D1}=0.009 μM and K_{D2}=0.091 μM). These data indicate
343 that this region of type 2 EBNA2 may adopt a different conformation to type 1 EBNA2 when
344 binding to $BS69_{CC\text{-}MYND.}$

345

346 In further experiments we addressed the impact of changing the serine at position 409 in type
347 2 EBNA2 to the aspartate present at the equivalent position (aspartate 442) in type 1 EBNA2on
348 BS69 binding in the context of the longer type 2 EBNA2 polypeptide containing three BS69
349 binding sites. To do this we expressed and purified a type 2 EBNA2 polypeptide with an S409D
350 mutation (T2 EBNA2$_{348-422}$ SD mutant). Interestingly, we found that the SD substitution
351 enhanced the detection of the second binding event on interaction with BS69$_{CC-MYND}$ (Figure
352 5C). The second binding event for T2 EBNA2$_{348-422}$ SD was associated with a larger change in
353 enthalpy (ΔH -7.65 kcal/mol) than the second binding event detected for T2 EBNA2$_{348-422}$ (ΔH
354 -1.59 kcal/mol) (Supplementary Table S2). Importantly we found that the affinities of the two
355 binding events remained largely unaffected (Figure 5B and C), consistent with our earlier
356 observations that the presence of serine at position 409 does not affect the ability of a type 2
357 polypeptide containing motif 1 and motif 2 to bind BS69 (Figure 1). To determine whether the
358 impact of the SD mutation was dependent on the presence of BS69 binding motif 3, we also
359 produced a polypeptide containing the SD and motif 3 mutation (EBNA2$_{348-422}$ SD + m3 mt).
360 We found that two binding events were still clearly detectable on interaction of this double
361 mutant type 2 EBNA2 polypeptide with BS69$_{CC-MYND}$ and that the enthalpy change of the
362 second binding event was similar to that of the single SD mutant (ΔH -9.62 kcal/mol)
363 (Supplementary Table S2) indicating that the impact of the SD change is still evident. The
364 affinity of the second binding event (K_{D2}) was however reduced by approximately 2-fold for
365 EBNA2$_{348-422}$ SD + m3 mt compared to the EBNA2$_{348-422}$ SD mutant (Figure 5C and D). These
366 data indicate that motif 3 contributes to the second binding event. We conclude that the SD
367 mutation previously shown to enhance the growth maintenance properties of type 2 EBNA2
368 (21) does not affect BS69 binding but likely alters the conformation of the type 2 EBNA2 TAD.
369 This may therefore impact on the binding of other transcriptional regulators that influence type
370 2 EBNA2 function.

371

372 *Full-length type 2 EBNA2 binds* $BS69_{CC\text{-}MYND}$ *more efficiently in pull-down assays*

373 To confirm our *in vitro* observations that a type 2 EBNA2 polypeptide binds an additional
374 BS69 dimer, we examined the interaction of $BS69_{CC\text{-}MYND}$ with full-length EBNA2 proteins
375 stably expressed in B cells. Lysates from cells expressing type 1 or type 2 EBNA2 or the type
376 2 SD mutant were incubated with recombinant GST-$BS69_{CC\text{-}MYND}$ immobilised on glutathione
377 beads for increasing times and the amount of EBNA2 precipitated determined by Western
378 Blotting (Figure 6). Consistent with the presence of an additional BS69 binding site in type 2
379 EBNA2, we found that GST-$BS69_{CC\text{-}MYND}$ pulled down type 2 EBNA2 more efficiently than
380 type 1 EBNA2 at short incubation times (Figure 6). In agreement with our *in vitro* observations
381 using the type 2 EBNA2 SD mutant, we found that this protein interacted with $BS69_{CC\text{-}MYND}$
382 with the same efficiency as type 2 EBNA2 (Figure 6). After 30 minutes incubation, GST-
383 $BS69_{CC\text{-}MYND}$ became saturated with EBNA2 and differences in association were no longer
384 evident. A control GST fusion protein (GST-Rab11) did not precipitate EBNA2, confirming
385 the specificity of the interactions. These data therefore confirm the increased association of
386 $BS69_{CC\text{-}MYND}$ with type 2 EBNA2.

387

388 *Mutation of BS69 binding motif 3 in type 2 EBNA2 increases its growth maintenance function*

389 To determine whether the presence of the additional BS69 binding motif in type 2 EBNA2
390 (motif 3) had functional consequences for the activity of type 2 EBNA2, we examined the
391 ability of a type 2 EBNA2 motif 3 mutant to maintain B cell growth. We utilised a previously
392 described assay using an EBV-infected LCL (EREB2.5) in which the activity of a type 1
393 estrogen receptor-EBNA2 fusion protein can be switched off by estrogen withdrawal (37). Loss
394 of EBNA2 activity leads to growth arrest, but transfection of a stably-maintained plasmid

395 expressing type 1 EBNA2 into these cells supports their survival (20). In contrast, the
396 expression of type 2 EBNA2 cannot maintain the growth of these cells (20). We found that
397 mutation of BS69 binding motif 3 produced a type 2 EBNA2 protein that was able to support
398 the recovery of these cells from the loss of type 1 EBNA2 activity, with cells recovering well
399 2-4 weeks following estrogen withdrawal (Figure 7A). The type 2 EBNA2 motif 3 mutant
400 behaved similarly to the type 2 EBNA2 SD mutant that was previously shown to support B cell
401 growth in this assay (21). We also examined the ability of the SD and motif 3 double mutant
402 in this assay and found that it showed a slightly increased ability to support B cells growth
403 (Figure 7A). In our hands, expression of type 1 EBNA2 supported initial growth in this assay
404 better than any type 2 mutants, with the mutants supporting growth recovery from 2 weeks
405 (Figure 7A). We confirmed that all EBNA2 proteins were expressed at similar levels (Figure
406 7B). We conclude that the presence of the additional BS69 binding motif in type 2 EBNA2
407 impairs the ability of type 2 EBNA2 to maintain B cell growth.

408

409 *A BS69 isoform containing the MYND domain is expressed in type 1 and type 2 EBV-infected*
410 *cells.*

411 BS69 functions as a negative regulator of EBNA2 transcription activity in reporter assays (34,
412 35), but previous studies have reported that BS69 expression is downregulated on infection of
413 resting B cells by EBV and is low in the resulting immortalised LCLs (35). Transcriptional
414 repression of BS69 by EBNA2 was implicated in BS69 downregulation indicating that EBNA2
415 may act to restrict expression of its own negative regulator (35). The cell lines examined in this
416 previous study all harboured type 1 EBV or type 1 EBNA2, so we next addressed whether
417 BS69 was expressed at similar levels in cells infected with type 1 and type 2 EBV. We
418 examined BS69 protein levels in type 1 and type 2 LCLs using an anti-BS69 antibody raised

419 against a region within the MYND domain of BS69. We found that BS69 was expressed at
420 similar levels in type 1 and type 2 LCLs, but surprisingly levels in LCLs were similar to those
421 in an EBV negative B cell line (AK31) (Figure 8A). We expanded our analysis to include
422 additional EBV negative B cell lines (BJAB and DG75), EBV infected cell lines displaying the
423 EBNA1 only latency I pattern of EBV gene expression (Akata and Mutu I), an additional type
424 1 LCL (IB4) and a BL cell line expressing all EBV latent proteins including EBNA2 (Mutu
425 III) (both latency III cell lines) (Figure 8B). We found no correlation between BS69 expression
426 and EBV infection or EBNA2 expression (Figure 8B). BS69 did not therefore appear to be
427 downregulated as a result of EBNA2 expression. We also examined BS69 expression over the
428 course of a primary B cell infection and found that BS69 was not downregulated as previously
429 reported (Figure 8C).

430

431 We therefore explored the possibility that we were detecting a different isoform of BS69.
432 Alternative splicing has been reported to give rise to different BS69 isoforms and four have
433 been experimentally verified (33) (Figure 9A). The canonical isoform (isoform 1, UniProt
434 identifier**:** Q15326-1) contains 15 exons and encodes a protein of 71 kD (602 amino acids).
435 Isoform 2 (Q15326-2) lacks amino acids 93-146 encoding the PHD domain (exon 4) and
436 encodes a protein of 64.4 kD. Isoform 3 (Q15326-3) lacks amino acids 563-602 encoding the
437 MYND domain (exon 15) and has a unique C-terminus encoded by an extended exon 14
438 sequence. Isoform 3 encodes a protein of 66.6 kD. Isoform 4 (Q15326-3) lacks exon 4 and
439 exon 15 (and thus both the PHD and MYND domains) and encodes a protein of 60 kD. These
440 isoforms were previously described as full length (FL), ΔPHD, ΔMD and ΔPHD, ΔMD
441 respectively (33), but the exon numbering used in this previous study differed. The BS69
442 protein detected in Figure 8A and B has a molecular weight of approximately 64 kD consistent
443 with that expected for isoform 2. This was the only protein detected by this antibody (against

444 the MYND domain), indicating that isoform 1 was not expressed in the cell lines examined.
445 Since the antibody we used would not detect BS69 isoforms 3 and 4, we could not exclude the
446 possibility that one or more of these isoforms was also expressed and that an alternative BS69
447 isoform was detected previously (35). In line with this possibility, we noted that the QPCR
448 analysis carried out by Harter *et al* used primers located in exon 4, which is absent from isoform
449 2.

450

451 No detail was provided on the anti-BS69 antibody used previously (35) and we were not able
452 to find another antibody that detected isoform 3 and 4 in Western blotting. We therefore took
453 a non-quantitative PCR approach to screen for different BS69 isoforms using cDNA prepared
454 from LCLs and from B cells during a primary EBV infection. PCR using a forward primer in
455 exon 3 and a reverse primer in exon 13 amplified two products indicating the presence of at
456 least two different isoforms, one containing exon 4 (1139 bps) and one lacking exon 4 (977
457 bps) (Figure 9B). This would be consistent with the presence of isoform 3 (which contains
458 exon 4) and isoform 2 (which lacks exon 4 and was detected by Western blotting (Figure 8)).
459 PCR products were sequenced to confirm their identity (data not shown). However, since
460 isoform 4 also lacks exon 4, this PCR analysis cannot rule out the additional presence of
461 isoform 4. Since in isoforms 3 and 4 exon 15 is replaced by a short unique 3' sequence from
462 exon 14, we designed reverse PCR primers in this unique 3' region. PCR using these primers
463 amplified only one product of 1578 bps consistent with presence of exon 4 and the unique 3'
464 region (isoform 3) (Figure 9B). The identity of this PCR product was again confirmed by
465 sequencing (data not shown). Importantly, we did not detect a smaller product (1416 bps) that
466 would indicate the presence of isoform 4 (lacks exon 4 and exon 15). Our data therefore
467 indicate that LCLs infected with either type 1 or type 2 EBV express both isoform 2 and
468 isoform 3 of BS69.

469

470 To quantitatively examine whether either BS69 isoform 2 or isoform 3 were downregulated on
471 EBV infection and in cells expressing EBNA2 as previously described (35), we used QPCR to
472 analyse BS69 mRNA expression in primary B cells infected by EBV and in a panel of EBV
473 negative and positive B cell lines. QPCR using primers that spanned exon 14 and exon 15
474 (present in isoform 1 and 2) detected variable levels of BS69 across the cell lines examined,
475 with no obvious correlation with EBV positivity or EBNA2 expression (present in latency III
476 EBV infected cell lines). This is consistent with the variability in BS69 protein expression
477 detected in Western blot analysis of isoform 2 expression (Figure 8). Although, in one
478 experiment (#2) primary B cells expressed high levels of BS69 isoform 2 mRNA that were
479 reduced on EBV infection, the second primary infection experiment did not reproduce this
480 observation. In fact, primary infection #2 was the same infection analysed by Western blotting
481 in Figure 8C so this change in BS69 RNA expression did not result in decreased expression of
482 BS69 isoform 2 protein. It is most likely therefore that BS69 isoform 2 expression varies in an
483 EBV and EBNA2 independent manner. Analysis of BS69 mRNA expression using QPCR
484 primers that would specifically amplify BS69 isoforms containing the long form of exon 14
485 (isoforms 3 and 4) also detected variable expression of BS69 that did not correlate with EBV
486 positivity or EBNA2 expression indicating that isoform 3 expression is also EBV independent
487 (Figure 9D).

488

489 We conclude that B cells infected with type 1 or type 2 EBV do not consistently display reduced
490 expression of any detectable isoform of BS69 compared to uninfected B cells. Since BS69
491 isoform 2 contains the MYND domain that binds EBNA2 (that is absent in isoform 3), the

492 continued expression of isoform 2 in EBV infected B cells would be expected to restrict the
493 gene activation function of EBNA2.

494

495 *Inhibition of BS69 function increases EBNA2 transactivation activity*

496 To determine whether inhibition of BS69 function increased EBNA2 transactivation function,
497 we carried out EBNA2 transactivation assays in an EBV negative B cell line (BJAB) in which
498 we overexpressed isoform 3 of BS69 lacking the MYND domain (ΔMYND) (but containing
499 the coiled-coil dimerisation domain). This form of BS69 has been proposed to act as a dominant
500 negative inhibitor of the MYND-domain dependent functions of BS69 (33). We performed
501 transactivation assays using EBNA2-GAL4-DNA binding domain (DBD) fusion proteins and
502 a Firefly luciferase reporter plasmid containing a synthetic promoter with 4 GAL4 binding
503 sites. Plasmids expressing GAL4-DBD fusion proteins containing regions of type 1 EBNA2
504 (334-487) and type 2 EBNA2 (301-454) encompassing all BS69 binding motifs were
505 transfected into BJAB cells in the presence or absence of plasmids expressing either full length
506 BS69 (isoform 1) or isoform 3 (ΔMYND). Consistent with previous reports, we found that
507 overexpression of full length BS69 inhibited transactivation by type 1 EBNA2 (34, 35) (Figure
508 10). BS69 also inhibited transactivation by type 2 EBNA2 (Figure 10). Consistent with its
509 function as a dominant negative inhibitor, we found that expression of BS69 ΔMYND
510 increased transactivation by both type 1 and type 2 EBNA2 (Figure 10). To determine whether
511 this was a non-specific or EBNA2-dependent effect, we expressed BS69 ΔMYND in the
512 absence of any GAL4-DBD-EBNA2 expressing constructs. In the absence of EBNA2 fusion
513 protein expression, BS69 ΔMYND had no effect on the activity of the GAL4 reporter (Figure
514 10). These data therefore demonstrate that inhibition of the MYND-domain dependent function
515 of BS69 in B cells relieves repression of EBNA2 transactivation. These data support our

516 hypothesis that the expression of MYND-domain containing BS69 isoforms in B cells impedes
517 EBNA2 gene activation function.
518
519 Taken together our *in vitro* and cell-based assays suggest that during initial B cell infection the
520 increased association of BS69 with type 2 EBNA2 may impede key gene activation events that
521 are required for the efficient outgrowth of immortalised cell lines.
522
523
524
525
526
527
528
529

530 **Discussion**

531 Type 2 EBV strains have reduced B cell transformation capacity and type 2 EBNA2 activates
532 some viral and cell genes less efficiently than type 1 EBNA2, a feature that may underlie the
533 impaired transformation phenotype. We have identified an additional binding site for the
534 transcriptional repressor BS69 in the EBNA2 protein encoded by type 2 strains of EBV and
535 show that mutation of this additional binding site improves the B cell growth maintenance
536 properties of type 2 EBNA2. Our data therefore implicate increased BS69 association in the
537 impaired function of type 2 EBNA2.

538

539 Type 2 EBV transforms resting B cells more slowly and results in the outgrowth of less
540 immortalised cell clones than type 1 EBV (1, 19). Although early type 2 EBV transformants
541 show reduced cell growth, the immortalised LCLs that eventually arise from a type 2 EBV
542 infection grow similarly to those infected with type 1 EBV. Type 2 LCLs also maintain similar
543 levels of expression of key EBNA2 target genes (20). This indicates that the impaired function
544 of type 2 EBNA2 restricts an early stage in the B cell transformation process *in vitro*. Indeed
545 two EBNA2 target genes that are only weakly activated by type 2 EBNA2 compared to type 1
546 EBNA2 (22), the viral oncogene LMP1 and the cell gene CXCR7, display slower and weaker
547 induction during primary infection with type 2 EBV (20). Although it was previously reported
548 that BS69 is downregulated on EBV infection, we found that there is continued expression of
549 BS69 isoform 2 in EBV-infected cells. Since this isoform contains the MYND domain that
550 mediates the BS69-EBNA2 interaction the expression of BS69 would be expected to restrict
551 EBNA2 activation function. Consistent with this prediction we found that the expression of a
552 dominant negative form of BS69 (isoform 3) lacking the MYND domain enhances EBNA2
553 activation function in B cells. Our data are consistent with a model where BS69 acts as a

554 restriction factor for both type 1 and type EBNA2 but the association of type 2 EBNA2 with
555 more molecules of the BS69 repressor protein further restricts the activation of growth and
556 survival genes important in early transformation. Why a small number of specific genes are
557 activated less well by type 2 EBNA2 is as yet not fully clear, but sequences resembling EICEs
558 (bound by ETS and IRF transcription factors) are found at EBNA2 binding sites in the LMP1
559 promoter and binding sites closest to the cell genes that show reduced activation by type 2
560 EBNA2. Interestingly BS69 binding to PXLXP motifs in ETS2 has been shown to inhibit its
561 transactivation activity (32). Since the ETS family member PU.1 is known to bind to the
562 putative EICE in the LMP1 promoter and plays a role in LMP1 promoter activation, it is
563 possible that type 2 EBNA2 functions less well in the context of PU.1 binding sites.
564 Interestingly, PU.1 also contains PXLXP motifs that would be predicted to bind BS69, so
565 enhanced tertiary complex formation between type 2 EBNA2, BS69 and PU.1 at the regulatory
566 elements of specific genes may function to stabilise BS69 binding and further restrict gene
567 activation by type 2 EBNA2.

568

569 Our data also provide important new molecular information on the nature of the complexes
570 formed between EBNA2 and BS69 that may applicable to the way BS69 interacts with other
571 cellular and viral transcription factors via its MYND domain. Single and multiple PXLXP
572 BS69 binding motifs have been identified in the cell and viral binding partners of BS69, but
573 the elucidation of the structure of the dimeric coiled-coil-MYND domain of BS69 led to a
574 model that proposed that a BS69 dimer bound to the two adjacent PXLXP motifs (motif 1 and
575 motif 2) in the same type 1 EBNA2 molecule (35). However, although the authors found that
576 BS69 bound with increased affinity when two PXLXP motifs were present in EBNA2
577 polypeptides, the three-dimensional structure obtained comprised a $BS69_{CC\text{-}MYND}$ dimer bound
578 to two separate type 1 EBNA2 motif 1 peptides. Although the binding of motif 1 and motif 2

579 could be accommodated in the $BS69_{CC\text{-}MYND}$ structure if the intervening 52 amino acids were
580 looped out, the formation of this complex has not been formally demonstrated (35). Our SEC-
581 MALS and SAXS analysis provides the first evidence that the $BS69_{CC\text{-}MYND}$ dimer
582 preferentially forms an intermolecular bridge between PXLXP motifs located on different
583 EBNA2 molecules. This mode of binding is consistent with the fact that EBNA2 is a dimeric
584 protein, with dimerisation mediated by the N-terminal END domain comprising amino acids
585 1-58 (36). Additional self-associating regions have also been mapped elsewhere in EBNA2
586 and include amino acids 97–121 and 122-344 (38, 39), although no molecular information is
587 available on how these regions may contribute to dimerisation. Our data indicate that BS69
588 binding to sites in the C-terminal transactivation domain may contribute to the formation or
589 stabilisation of EBNA2 dimers. Interestingly, although SEC analysis clearly demonstrated
590 complex formation between both type 1 and type 2 EBNA 2 polypeptides and $BS69_{CC\text{-}MYND,}$
591 the elution profiles of both complexes were broad. The type 1 EBNA2-$BS69_{CC\text{-}MYND}$ elution
592 profile had a clear shoulder indicating the presence of smaller MW complexes (Figure 3A).
593 This would explain why the average MW determined by SEC-MALs was smaller than expected
594 for a complex that contained two molecules of type 1 EBNA2 and two $BS69_{CC\text{-}MYND}$ dimers.
595 It is possible that in solution *in vitro* there is a mixed population of dimeric type 1 EBNA2 and
596 monomeric type 1 EBNA2 complexes (where a single EBNA2 polypeptide is bound by one
597 $BS69_{CC\text{-}MYND}$ dimer as previously proposed). We were not able to investigate this further using
598 SAXS as this 'shoulder' was not clearly defined, so SAXS analysis for both type 1 and type 2
599 EBNA2-BS69 complexes focused on the major elution peak of the large complex. Given that
600 full length EBNA2 expressed in EBV-infected cells is a dimer, complexes involving two
601 EBNA2 molecules are more likely to be physiologically relevant.

602

603 Surprisingly, in our GAL4-EBNA2 fusion protein assays we did not see weaker transactivation
604 by the type 2 EBNA2 fusion protein compared to the type 1 EBNA2 fusion protein as reported
605 previously (21). We used a longer region of EBNA2 compared to this previous study that
606 encompassed all three BS69 binding sites for type 2 EBNA2 and the corresponding region of
607 type 2 EBNA2 (with only two functional BS69 binding sites). Previously GAL4-EBNA2
608 fusion protein constructs were used that expressed a type 1 EBNA2 protein containing only
609 BS69 binding motif 2 or the corresponding region of type 2 EBNA2 that contained BS69
610 binding motif 2 and 3 (21). It is not completely clear why the increased association of BS69
611 with type 2 EBNA2 is not associated with weaker transactivation in our assays in the context
612 of a longer region of EBNA2, but it could point to the importance of the dimerisation that
613 occurs in the context of the full-length protein in the assembly of larger BS69-EBNA2
614 complexes.
615

616 When considering the nature of assembly of BS69-EBNA2 complexes, it is likely that binding
617 to motif 1 (which in type 1 EBNA2 has the highest affinity for $BS69_{CC\text{-}MYND}$) would drive the
618 initial interaction between EBNA2 and BS69 and binding to motif 1 probably constitutes the
619 first binding event that can be distinguished in our ITC analysis using an increased number of
620 injections. For type 2 EBNA2, since both motif 2 and 3 bind BS69 with similar affinity, binding
621 to both of these motifs probably occurs with similar kinetics and is detectable as a single second
622 binding event by ITC. Given the fact that $BS69_{CC\text{-}MYND}$ dimers are predicted in the solution
623 structure of the BS69-EBNA2 complex to be located side by side along a dimeric EBNA2
624 molecule, it is possible that interactions between BS69 coiled-coil dimers play a role in
625 stabilising the oligomeric complex.

626

627 Our initial interest in examining type-specific binding of EBNA2 to BS69 centred around the
628 influence of a serine residue in the TAD of type 2 EBNA2 that plays a key role in restricting B
629 cell growth maintenance by type 2 EBNA2 (21). Although this residue is located immediately
630 adjacent to BS69 binding motif 2 in type 2 EBNA2, we found that it did not increase BS69
631 binding (as might have been expected) when binding was compared to the corresponding
632 region of type 1 EBNA2 where there is an aspartate residue in its place. It does not appear
633 therefore that the influence of serine 409 on growth maintenance is mediated through
634 alterations in BS69 binding affinity. Our ITC analysis however did find that a serine to
635 aspartate change at this position in type 2 EBNA2 altered the nature of BS69 binding indicating
636 that it may induce a conformational change in this region of EBNA2. This could result in
637 differences in the binding of other transcription regulators to the type 2 EBNA2 TAD compared
638 to the type 1 EBNA2 TAD. Possibilities could include increased binding of a repressor or co-
639 repressor to the type 2 EBNA2 TAD or decreased binding of an activator or co-activator.

640

641 BS69 may have a wider role in regulating B cell transformation and the growth of EBV-
642 infected cells in addition to its modulation of EBNA2 transactivation. BS69 localised to the
643 cell membrane has also been implicated as an adaptor in signalling mediated by the EBV
644 oncogene LMP1. The MYND domain of BS69 was reported to bridge an interaction between
645 the carboxy terminal cytoplasmic domain of LMP1 and the TRAF6 signalling protein to
646 activate the JNK signalling pathway (40). Conversely, BS69 has also been implicated as a
647 negative regulator of LMP1-mediated NF-κB signalling by decreasing the association between
648 C-terminal activation region (CTAR) 2 of LMP1 and the signalling adaptor TRADD (41) and
649 by binding to CTAR1 and bringing in the negative regulator of NF-κB signalling, TRAF3 (42).
650 Although further work appears to be required to fully understand the role of BS69 in LMP1
651 signalling and the relative proportions of nuclear and membrane-associated BS69, it is possible

652 that BS69 is a key modulator of growth promoting events in EBV-infected cells. In this context,
653 our work now sheds new light on how transformation by type 2 strains of EBV may be
654 specifically curbed as a result of sequence variation that results in the creation of an additional
655 binding site for BS69.

656

657 **Materials and Methods**

658 *Cell lines*

659 All cell lines were passaged twice weekly in RPMI 1640 media (Invitrogen) supplemented with
660 10% Fetal Bovine serum (Gibco), 1 U/ml penicillin G, 1 µg/ml streptomycin sulphate and 292
661 µg/ml L-glutamine at 37°C in 5% CO_2. DG75 (43) and AK31 (44) are EBV negative BL cell
662 lines and BJAB (45) is an EBV negative B cell lymphoma line. Akata (46) and Mutu I are EBV
663 positive latency I BL cell lines and Mutu III is a cell line derived from Mutu I cells that drifted
664 in culture to express all EBV latent proteins (latency III) (47). All LCLs also display the latency
665 III pattern of EBV gene expression and were described previously (48); IB4, spLCL, LCL3,
666 C2 + Obaji, JAC-B2, BM + Akata LCLs are infected with type 1 EBV and C2 + BL16, WEI-
667 B1, Jijoye and AFB1 LCLs are infected with type 2 EBV. The ER-EB 2.5 LCL, expressing a
668 conditionally active oestrogen receptor (ER)-EBNA2 fusion protein, was provided by Prof B.
669 Kempkes and was cultured in the presence of β-estradiol (37). The Daudi:pHEBo-MT:E2T1,
670 Daudi:pHEBo-MT:E2T2 and Daudi:pHEBo-MT:E2T2 S442D cell lines were generated and
671 cultured as described previously (21). B cell infection samples were described previously (49).

672

673 *Plasmids*

674 Constructs expressing N-terminal 6 x histidine tagged EBNA2 polypeptides were generated
675 using the Sequence and Ligation Independent Cloning (SLIC) technique using type 1 EBNA2
676 (B95-8), type 2 EBNA2 (AG876) and type 2 EBNA2 SD (serine to aspartate at position 409)
677 pSG5 expression plasmids as templates to amplify the regions of interest. DNA was PCR
678 amplified using primers containing 20-30 bp of additional sequence from the regions 5' and 3'
679 to the multiple cloning site of pET47b+. pET47b+ was digested using SmaI and HindIII and
680 the PCR product and double-digested vector were then partially digested using the 3' to 5'
681 exonuclease activity of T4 DNA Polymerase in the absence of dNTPs to generate long

682 complementary 5' overhangs. The PCR products and pET47b+ were then annealed on ice. The
683 ligated DNA fragments obtained contain four nicks that are repaired by *E. coli* after
684 transformation. For type 1 EBNA2, constructs encoded amino acids 381-445 or 381-455 to
685 generate pET47b+ T1 EBNA2$_{381-445}$ and pET47b+ T1 EBNA2$_{381-455.}$ Type 2 EBNA2 constructs
686 encoded amino acids 348-412 or 348-422 to generate pET47b+ T2 EBNA2$_{348-412,}$ pET47b+ T2
687 EBNA2$_{348-422}$ and pET47b+ T2 EBNA2$_{348-422}$ SD.
688 The BS69 CC-MYND domain (amino acids 480-602) was amplified from pCI-BS69
689 containing the full length human BS69 sequence (gift from Dr Stéphane Ansieau) and cloned
690 using SLIC into the SmaI and HindIII sites of pET49b+ to generate a construct expressing an
691 N-terminal GST-6x Histidine tag BS69$_{CC-MYND}$ fusion protein.
692 To create GAL4-DNA-binding domain-EBNA2 TAD fusion protein expressing constructs
693 pBlueScript plasmids carrying EBNA2 sequences were used as the template to PCR amplify
694 the type 1 EBNA2 TAD (amino acids 426-463) and the type 2 EBNA2 TAD (amino acids 334-
695 487) using *Taq* DNA polymerase. Primers contained *Bam*HI or *Not*I restriction sites at their 5'
696 ends. PCR products were first cloned into pCR2.1 using the TA cloning kit (Invitrogen)
697 according to the manufacturer's instructions. The pCR2.1 vector carrying the cloned PCR
698 product was then digested with *Bam*HI and *Not*I and the EBNA2 TAD fragment then cloned
699 into the *Bam*HI and *Not*I sites of pcDNA3.1-GAL4-DBD.
700
701 *Site-directed mutagenesis*
702 Reverse PCR with the Q5® Site-Directed Mutagenesis kit (NEB) was used to introduce
703 mutations into BS69 binding motif 3 in the pET47b+ T2 EBNA2$_{348-422}$ construct. This resulted
704 in a change from PTLEP to ATAEA and generated pET47b+ T2 EBNA2$_{348-422}$ motif 3 mt. The
705 same primers were used to mutate motif 3 in the context of the SD mutation to generate
706 pET47b+ T2 EBNA2$_{348-422}$ SD + motif 3 mt.

707

708 *Growth maintenance assay*

709 The EREB2.5 growth assay was performed as described previously (20). Briefly, 5 µg of OriP-
710 p294 plasmids expressing type 1 EBNA2, type 2 EBNA2 or type 2 EBNA2 mutants were
711 transfected into 5 × 10^6 EREB 2.5 cells resuspended in 110 µl of buffer T using Neon
712 transfection with 1 pulse of 1300 V for 30 msec. Following transfection, cell suspensions were
713 added to 2 ml of media supplemented with 10% FBS and antibiotics but without β-oestradiol
714 and incubated overnight in 12-well plates. The following day each transfected sample was
715 made up to 10 mls with media and divided into 5 x 2 ml aliquots in a 12-well plate. Samples
716 were harvested for cell counting and protein analysis at time points up to 4 weeks.

717

718 *Reporter assays*

719 Cells were diluted 1:3 in fresh culture medium one day before transfection. 2 x 10^6 BJAB cells
720 were used for each individual transfection. Cells were pelleted by centrifugation at 335*g* for 5
721 minutes at 4ºC and washed twice with pre-warmed PBS. Cells were resuspended in 100 µl of
722 Neon resuspension solution R (Invitrogen). Cell suspensions were then mixed with plasmid
723 DNA (2-12 µg in TE buffer). Cells were co-transfected with 300 ng of either type 1 GAL4-
724 DBD:EBNA2 (aa 334-487) or type 2 GAL4-DBD:EBNA2 (301-454) constructs, 500 ng of
725 pFRLuc (Agilent technologies), 10 ng of pRL-CMV (Promega) and 1 µg of BS69 (pCI-BS69)
726 or BS69 ΔMYND (pCI-BS69-ΔMYND) expressing plasmids (gift from Dr Stéphane Ansieau).
727 The DNA and cell mixture was transferred to a 100 µl Neon transfection pipette tip
728 (Invitrogen). Cells were electroporated using Neon transfection protocol 14 (1200 V of pulse
729 voltage, 20 ms of pulse width and 2 pulse number) and then transferred into 2 ml of pre-warmed
730 media in a 6-well plate and incubated at 37ºC for 24 hr.

731 Cell pellets were then lysed using 100 µl of 1X Passive Lysis buffer (Promega). Two freeze-
732 thaw cycles were performed to achieve efficient lysis (20 sec on dry ice and thawing at room
733 temperature for 2 min). Cell debris was removed by centrifugation at 25,000*g*, for 1 min at 4ºC
734 and the clear supernatant was then transferred to a fresh tube. 20 µl of lysate was assayed for
735 firefly and Renilla luciferase activity using 20 µl of each dual luciferase assay kit reagent
736 (Promega) and a microplate luminometer (LUMIstar Omega, BMG Labtech).
737
738 *Recombinant protein production*
739 pGEX4T1-BS69 (kindly provided by Dr Stéphane Ansieau) was used to express a GST-BS69
740 fusion protein containing amino acids 452-602 of BS69 encompassing the CC-MYND
741 domain (numbered according to the canonical isoform) (34). pGEX4T1-RAB11B expressing
742 GST-tagged RAB11B (gift from Prof Gill Elliott) was used to produce a negative control
743 protein for the GST pull-down assays.

744 For production of $BS69_{CC\text{-}MYND}$ and EBNA2 polypeptides, the relevant plasmids were
745 transformed into the Rosetta 2 (DE3) pLysS E. Coli strain and protein expression induced by
746 adding 0.4 mM of isopropyl βD-1-thiogalactopyranoside (IPTG) to 3 litre cultures at an
747 OD_{600nm} of 0.6. The bacteria were then grown at 20°C overnight before harvesting for protein
748 purification. Cell pellets from a 3 litre induced culture were lysed for 30 minutes on ice with
749 constant stirring in 100 ml of lysis buffer (25 mM Tris-HCL pH 7.5, 500 mM NaCl, 5%
750 Glycerol). The lysis buffer was supplemented with 0.25 mg/ml lysozyme, 2 mM $MgCl_2$, 1 mM
751 TCEP (tris(2-carboxyethyl)phosphine), two protease-inhibitor complete tablets (Roche) and
752 DNase and 0.2 mg/ml of DNase I. Lysates were then sonicated at 37% amplitude for 5 minutes
753 with 10 seconds pulses using a Vibra-cell sonicator (SONICS). The cell debris was pelleted at
754 15000 rpm for 45 minutes at 4°C (Biofuge Stratos, Heraeus). Beads from 3 ml of HisPur™
755 Cobalt Resin slurry (Thermo Scientific) were added to the cleared lysate along with 2 mM

756 imidazole and the sample incubated for 1 hour and 30 minutes at 4°C with rolling. Samples
757 were decanted into a centrifuge column (Thermo Scientific Pierce) and washed with buffer
758 (25mM Tris-HCl, 500mM NaCl and 1mM TCEP, 2 mM of imidazole, pH 7.5). The protein
759 was eluted from the beads using buffer containing increasing concentrations of imidazole (5
760 mM, 10 mM, 20 mM, 50 mM, 100 mM, 200 mM, 300 mM and 500 mM). Fraction samples
761 were analysed by SDS-PAGE and the fractions containing recombinant protein were pooled
762 and incubated with 3C protease (200 µl of 2 mg/ml) in the presence of 2 mM DTT overnight
763 at 4°C to cleave the Histidine tag. His-tag cleaved proteins were then separated from the 3C
764 protease by passing the protein sample through a GSTrap HP column (Amersham) using a
765 peristaltic pump to capture the GST-tagged 3C protease. Untagged recombinant proteins were
766 then concentrated and injected into a HiLoad™ 16/600 Superdex™ 75g Column (GE
767 Healthcare) pre-equilibrated in 25 mM Tris-HCL, 200 mM NaCl, 1 mM TCEP, pH 7.5 purified
768 at 0.5 ml/min. Protein fractions containing purified protein were then pooled, concentrated and
769 stored at -80°C until required. Approximately 1 mg of purified EBNA2 polypeptides or 4 mg
770 of $BS69_{CC\text{-}MYND}$ was obtained from 1 litre of culture.
771
772 *Isothermal titration calorimetry*
773 Four commercially synthesized peptides (Peptide Synthetics) were used for ITC. These
774 included BS69 binding motif 2 of type 1 EBNA2 (435-445) or type 2 EBNA2 (402-412) and
775 putative BS69 binding motif 3 of type 1 EBNA2 (445-455) or type 2 EBNA2 (412-422).
776 Frozen protein was quickly thawed using running water and dialysed overnight at 4°C using
777 Slide-A-Lyzer® MINI Dialysis Units (Thermo Scientific) against ITC buffer (20mM Tris-HCl,
778 100mM NaCl and 1mM TCEP , pH 7.5). The next day, protein samples were centrifuged at
779 13000 rpm for 10 minutes at 4ºC and the concentration was determined by NanoDrop
780 spectroscopy (NanoDrop Technologies) with their respective molecular weights and extinction

781 coefficients. EBNA2 peptides (1mM) and polypeptides (type 1, 0.3 mM and type 2, 0.6 mM)
782 were titrated against $BS69_{CC\text{-}MYND}$ (0.1mM) at 25°C using a MicroCalTM iTC200 instrument
783 (Malvern). For peptides, 13 x 3.0 µl injections were used for titration. For EBNA2 polypeptides
784 19 x 2.0 µl or 29 x 1.3 µl injections were used for titration. ITC data were corrected for non-
785 specific heat and analysed using MicroCal Origin® 7.0. The experiments were performed in
786 triplicate alongside a control experiment with no $BS69_{CC\text{-}MYND}$ (buffer only in the cell). All
787 polypeptides were used within 24 hours of dialysis into ITC buffer.
788
789 *Size Exclusion Chromatography*
790 An S200 10/300 GL gel filtration column (GE Healthcare) was equilibrated with buffer
791 containing 20mM Tris-HCl, 100mM NaCl and 1mM TCEP, pH 7.5. Individual EBNA2 or
792 $BS69_{CC\text{-}MYND}$ polypeptides or complexes were applied to the column and analysed at a flow
793 rate of 0.5ml/min. The eluted fractions were then analysed by SDS-PAGE and Quick
794 Coomassie staining.
795
796 *Size Exclusion Chromatography-multi-angle light scattering*
797 EBNA2-BS69 complexes were prepared by pre-incubating proteins in a 1:3 molar ratio for at
798 least 30 mins at 4°C. Purified samples (45 µl) at a concentration of 5 mg/ml were loaded onto
799 a Shodex KW403-4F column at 25°C pre-equilibrated in 20 mM Tris-HCl, 100mM NaCl and
800 1mM TCEP, pH 7.5. Elution fractions were monitored using a DAWN HELEOS II MALS
801 detector followed by a refractive index detector Optilab T-rEX (Wyatt Technology). Molecular
802 masses of each individual peak were determined using ASTRA 6 software (Wyatt
803 Technology). For normalization of the light scattering and data quality, BSA was used as a
804 calibration standard.

805 *Small-angle X-ray scattering*

806 Synchrotron radiation X-ray scattering data from solutions of individual proteins or complexes
807 prepared as for SEC-MALS were collected on beamline B21 at Diamond Light Source (Didcot,
808 United Kingdom), with an inline HPLC system. X-ray scattering patterns were recorded on a
809 Pilatus detector after injection of 45 µl of protein sample (5-10 mg/ml) in a Superdex 200
810 3.2/300 column equilibrated in 20mM Tris-HCl, 100mM NaCl, 2% Sucrose and 1mM TCEP,
811 pH 7.5. Samples were analysed at 20°C using a flow-rate of 0.25 ml/min. Initial data processing
812 (background subtraction and radius of gyration Rg calculation) was performed using ScÅtter
813 (v3.0 by Robert P. Rambo; Diamond Light Source). *Ab initio* beads model for the complex
814 were prepared using DAMMIF (50). 23 independent dummy atom models were obtained by
815 running the program in 'slow' mode. DAMAVER was then used to align and average the
816 models (51). The *ab initio* generated beads models were refined using DAMMIN and compared
817 to the experimental scattering data to derive χ^2 values (52). The goodness-of-fit χ^2values for the
818 docked structure compared to the experimental scattering data were determined with FoXS
819 (53).

820 *GST pull-down assays*

821 Nuclear extracts were prepared from control or EBNA2 expressing Daudi cell lines. EBNA2
822 expression in Daudi:pHEBo-MT:EBNA2 cells was induced with 5 µM $CdCl_2$ for 24 hours. At
823 least $4x10^7$ cells were then harvested and resuspended in 1 ml of buffer A (10 mM HEPES pH
824 7.9, 1.5 mM MgCl2, 10 mM KCl, 0.5 mM 1,4-dithiothreitol (DTT) (Sigma), 1 mM PMSF
825 (Sigma) and 1x complete protease inhibitor cocktail (Roche)). Cells were pelleted by
826 centrifugation at 1000*g* for 5 min at 4ºC and lysed in 100 µl of buffer A supplemented with
827 0.1% (v/v) NP-40 and incubated on ice for 5 min. Cell lysates were centrifuged at 2700*g* for
828 30 sec at 4ºC and the nuclei resuspended in 50 µl of buffer B (20 mM HEPES pH 7.9, 420 mM
829 NaCl, 1.5 mM MgCl2, 0.2 mM EDTA, 1 mM PMSF, 25% (v/v) glycerol, 1 mM DTT and 1x

830 complete protease inhibitor cocktail) at 4ºC for 20 min with rotation. Samples were finally
831 centrifuged at 11,600*g* for 10 min at 4ºC and the supernatants/nuclear extracts were transferred
832 to fresh eppendorf tubes and the protein concentration was determined before storage at -80ºC.

833

834 Lysates containing GST-tagged $BS69_{CC\text{-}MYND}$ or GST-RAB11B were prepared from 100 ml
835 cultures of E. Coli BL21 (DE3). Transformed cells were cultured at 30ºC until they reached an
836 OD_{600nm} of 0.6 and protein expression was induced at 25ºC with 0.5 mM IPTG for 3-4 h. Cells
837 were pelleted at 2,800*g* for 20 min at 4ºC and then resuspended in 10 ml of Lysis buffer (20
838 mM Tris-Cl pH 8.0, 150 mM NaCl and 1 mM DTT) supplemented with 120 µl of lysozyme
839 (10 mg/ml) and lysates incubated on ice for 20 min. Lysates were sonicated at high speed for
840 3 x 15 sec pulses in ice water using an Ultrasonic XL2020 Processor (Heat Systems) and cell
841 debris pelleted at 17,900*g* for 30 min at 4ºC. Lysates were stored at -80ºC until required.

842

843 For pull-down assays, 50 µl of 50% Glutathione-Sepharose 4B Bead slurry (GE Healthcare)
844 was washed three times in ice-cold binding buffer (20 mM Tris-Cl pH 8.0, 150 mM NaCl, 1
845 mM DTT and 0.1 mg/ml BSA). Beads were pelleted by centrifugation at 25,000*g* for 1 min
846 and 100 µl of bacterial lysate containing the GST-tagged protein was incubated with the washed
847 beads for 1 h at 4ºC with rotation. Glutathione-Sepharose Beads bound to the GST-tagged
848 protein were then washed with ice-cold binding buffer six times and pelleted by centrifugation
849 at 25,000*g* for 1 min. Loaded GST- $BS69_{CC\text{-}MYND}$ beads were then incubated with nuclear
850 extracts containing EBNA2 at 4ºC for different times (5, 10 and 30 minutes). Loaded GST-
851 RAB11B beads were incubated with lysates for 30 minutes. Beads were then washed six times
852 with ice-cold binding buffer and pelleted by centrifugation at 25,000*g* for 1 min. Beads were
853 then resuspended in 25 µl of 2x SDS sample buffer (120 mM Tris-Cl pH 6.8, 4% (w/v) SDS,

854 2% (v/v) β-mercaptoethanol, 20% (v/v) glycerol and 0.01% (w/v) bromophenol blue) and
855 incubated at 95ºC for 5 min and analysed for EBNA2 levels by SDS-PAGE and Western
856 blotting.
857
858 *SDS-PAGE and Western blotting*
859 SDS-PAGE and Western blotting was carried out as described previously (54, 55) using the
860 anti-EBNA2 monoclonal antibody PE2 (gift from Prof M. Rowe) anti-actin 1/5000 (A-2066,
861 Sigma) and anti-BS69 1/1000 (ab190890, Abcam). Western blot visualisation and signal
862 quantification was carried out using a Li-COR Imager. Gels were stained using Quick
863 Coomassie stain (Generon Ltd).
864
865 *PCR and QPCR*
866 RNA was extracted from cells using Trireagent (Sigma), further purified using the RNeasy kit
867 (Promega) and cDNA synthesised using random primers and the ImProm II reverse
868 transcription kit (Promega). Standard PCR reactions were performed with Phusion DNA
869 polymerase (New England Biolabs) using the relevant BS69 primers listed in Supplementary
870 Table S1. Quantitative PCR was performed in duplicate using the standard curve absolute
871 quantification method on an Applied Biosystems 7500 real-time PCR machine as described
872 previously (56) using the relevant primers listed in Supplementary Table S1. The efficiency of
873 all primers was determined prior to use and in each experiment and all had amplification
874 efficiencies within the recommended range (90–105%).
875
876 **Data Availability**
877 SAXS data have been deposited in the small angle scattering biological data bank (SASBDB)

878 (www.sasbdb.org) under accession numbers SASDEF6, SASDEG6, SASDEH6, SASDEJ6,
879 SASDEK6;
880 https://www.sasbdb.org/data/SASDEF6/5llm1wasc4/
881 https://www.sasbdb.org/data/SASDEG6/4yff1ro01u/
882 https://www.sasbdb.org/data/SASDEH6/tpia09j2m0/
883 https://www.sasbdb.org/data/SASDEJ6/werm0avk55/
884 https://www.sasbdb.org/data/SASDEK6/07t9uflv7k/
885

886 **Acknowledgements**

887 We thank Dr Stéphane Ansieau and Prof Gill Elliott for providing plasmids. We thank
888 Diamond Light Source for beamtime (proposal mx14891) and the staff of beamline B21 for
889 assistance with data collection.

890

891

892

893 **Figure Legends**

894 **Figure 1. Isothermal titration calorimetry analysis of the interaction of type 1 and type 2**
895 **EBNA2 peptides and polypeptides containing BS69 binding motif 2 with BS69$_{CC\text{-}MYND}$.**
896 (A) Amino acid sequence of the regions of type 1 (B95-8) and type 2 (AG876) EBNA2
897 containing BS69 binding motifs 1 and 2 (underlined). Asterisks show the positions of the P, L
898 and P amino acids in the PXLXP binding motif. Aspartate 442 in type 1 EBNA2 and the
899 corresponding serine 409 in type 2 EBNA2 adjacent to motif 2 are shown in red. (B) Isothermal
900 titration calorimetry (ITC) analysis of type 1 EBNA2 motif 2 peptide binding to BS69$_{CC\text{-}MYND}$.
901 The upper panel shows heat peak data as Differential Power (DP) versus time and the lower
902 panel shows ΔH (derived from integration of the heat peak intensities) plotted against the
903 BS69$_{CC\text{-}MYND}$/EBNA2 molar ratio (based on monomer concentrations). Titrations were
904 performed using a series of 13 2.0 µl injections of 1 mM EBNA2 peptide and 0.1 mM BS69$_{CC\text{-}}$
905 $_{MYND}$ in the cell. The solid line shows the best fit using a one-site (one event) binding model
906 with the n value fixed to 1. The dissociation constant (K_D) displayed shows the mean ± standard
907 deviation obtained from 3 independent experiments (C) ITC analysis of the binding of the type
908 1 EBNA2 polypeptide T1 EBNA2$_{381\text{-}445}$ (0.6 mM) to BS69$_{CC\text{-}MYND}$ using 19 2.0 µl injections
909 of 0.1 mM EBNA2 polypeptide. The n value indicates the stoichiometry of BS69$_{CC\text{-}}$
910 $_{MYND}$/EBNA2 binding calculated for monomeric proteins and shows the mean ± standard
911 deviation from 3 independent experiments. (D) ITC analysis of the binding of the type 2
912 EBNA2 polypeptide T2 EBNA2$_{348\text{-}412}$ (0.3 mM) to BS69$_{CC\text{-}MYND}$ (0.1 mM) as in C.

913

914

915 **Figure 2. Isothermal titration calorimetry analysis of the interaction of type 1 and type 2**
916 **EBNA2 peptides and polypeptides containing BS69 binding motif 3 with BS69$_{CC\text{-}MYND}$.**

917 (A) Amino acid sequence of the regions of type 1 (B95-8) and type 2 (AG876) EBNA2
918 containing BS69 binding motifs 1, 2 and 3 (underlined). Asterisks show the positions of the P,
919 L and P amino acids in the PXLXP binding motif. (B) Isothermal titration calorimetry (ITC)
920 analysis of type 1 EBNA2 motif 3 peptide binding to $BS69_{CC\text{-}MYND}$ (no binding was detected
921 so the K_D could not be determined (n.d.). (C) Isothermal titration calorimetry (ITC) analysis of
922 type 2 EBNA2 motif 3 peptide binding to $BS69_{CC\text{-}MYND}$ using 19 injections of 2.0 µl EBNA2
923 peptide. Data are displayed and analysed as in Figure 1. (C) ITC analysis of the binding of type
924 2 EBNA2 motif 3 peptide binding to $BS69_{CC\text{-}MYND}$ as in B. (D) ITC analysis of the binding of
925 the type 1 EBNA2 polypeptide $EBNA2_{381\text{-}455}$ to $BS69_{CC\text{-}MYND.}$ (E) ITC analysis of the binding
926 of the type 2 EBNA2 polypeptide T2 $EBNA2_{348\text{-}422}$ to $BS69_{CC\text{-}MYND}$. (F) ITC analysis of the
927 binding of the type 2 EBNA2 polypeptide T2 $EBNA2_{348\text{-}422}$ with BS69 binding motif 3 mutated
928 from PTLEP to ATAEA.

929

930 **Figure 3. Solution state analysis of EBNA2 and $BS69_{CC\text{-}MYND}$ complexes.** (A) Size exclusion
931 chromatography of individual type 1 and type 2 EBNA2 polypeptides, $BS69_{CC\text{-}MYND}$ and
932 EBNA2-$BS69_{CC\text{-}MYND}$ complexes. Absorbance was normalized to the type2 EBNA2-BS69
933 complex (highest absorbance) using UNICORN software. (B) Samples from the indicated
934 fractions were analysed by SDS-PAGE followed by Coomassie staining.

935

936 **Figure 4. Solution structure of EBNA2-$BS69_{CC\text{-}MYND}$ complexes determined by SAXS.** (A)
937 SAXS scattering data for type 1 $EBNA2_{381\text{-}455}$-$BS69_{CC\text{-}MYND}$ (black dots) fitted to the *ab initio*
938 DAMMIN dummy atom model (red line). SAXS scattering data fitted to the docked structural
939 complex shown in B (green) with the χ^2 determined by FoXS. Plots show relative log intensity
940 vs scattering vector (q). (B) Solution structure of type 1 $EBNA2_{381\text{-}455}$-$BS69_{CC\text{-}MYND.}$ The

941 SAXS envelopes (grey mesh) were generated by averaging 23 *ab-initio* models using the
942 DAMMIF programme. The crystal structures of two $BS69_{CC\text{-}MYND}$ dimers (PDB ID: 5HDA)
943 are shown in cyan and were manually docked into the SAXS envelope along with the *ab-initio*
944 dummy atom SAXS solution structures of two type 1 $EBNA2_{381\text{-}455}$ polypeptides (salmon). The
945 maximum dimension (D_{max}) and volume were calculated using ScÅtter. (C) SAXS scattering
946 data for type 2 $EBNA2_{348\text{-}422}$-$BS69_{CC\text{-}MYND}$ (black dots) fitted to the *ab initio* DAMMIN
947 dummy atom model (red line). SAXS scattering data fitted to the docked structural complex
948 shown in D (green) with the χ^2 determined by FoXS. (D) Solution structure of type 2
949 $EBNA2_{348\text{-}422}$-$BS69_{CC\text{-}MYND}$ obtained as described in (B). The crystal structures of three
950 $BS69_{CC\text{-}MYND}$ dimers (PDB ID: 5HDA) are shown in cyan and were manually docked into the
951 SAXS envelope along with the *ab-initio* dummy atom SAXS solution structures of two type 2
952 $EBNA2_{348\text{-}422}$ polypeptides (orange).

953

954 **Figure 5. Isotheral titration calorimetry analysis of the interaction of type 1 and type 2**
955 **EBNA2 polypeptides with $BS69_{CC\text{-}MYND}$ using an increased number of injections**. **(**A) ITC
956 analysis of the binding of the type 1 EBNA2 polypeptide $EBNA2_{381\text{-}455}$ to $BS69_{CC\text{-}MYND.}$
957 Titrations were performed using a series of 29 injections of 1.3 µl 0.3 mM EBNA2 polypeptide
958 and 0.1 mM $BS69_{CC\text{-}MYND}$ in the cell. The solid line shows the best fit using a two-site (two
959 event) binding model. The mean dissociation constant (K_D) ± standard deviation from 3
960 independent experiments is shown for each binding event. (B) ITC analysis of the binding of
961 the type 2 EBNA2 polypeptide T2 $EBNA2_{348\text{-}422}$ to $BS69_{CC\text{-}MYND}$ using 29 injections and fitting
962 using a two-site (two event) binding model as in A. (C) ITC analysis of the binding of the type
963 2 EBNA2 polypeptide T2 $EBNA2_{348\text{-}422}$ SD containing the serine 412 to aspartate mutation
964 using 29 injections and fitting using a two-site (two event) binding model. (D) ITC analysis of
965 the binding of the type 2 EBNA2 polypeptide T2 $EBNA2_{348\text{-}422}$ with BS69 binding motif 3

966 mutated from PTLEP to ATAEA using 29 injections and fitting using a two-site (two event)
967 binding model.

968 **Figure 6.** GST pulldown assay using GST-BS69$_{CC-MYND}$ and lysates from B cell lines
969 expressing type 1 and type 2 EBNA2. Nuclear extracts of Daudi:pHEBo-MT:EBNA-2 cells
970 expressing type 1 (T1), type 2 (T2) or type 2 SD EBNA2 proteins were incubated for 5, 15 or
971 30 min at 4ºC with glutathione beads which had been loaded with bacterial lysates expressing
972 the GST- BS69$_{CC-MYND}$. GST-RAB11B was used as a negative control and was incubated for
973 30 min with the nuclear extracts. Following washing, beads were resuspended in protein sample
974 buffer and analysed by SDS-PAGE and Western blotting for EBNA2 using the PE2 anti-
975 EBNA2 antibody. The EBNA2 proteins expressed by these cell lines display almost the same
976 size (72 kD) since the number of polyproline residues had been equalised in all the EBNA2
977 alleles.

978

979 **Figure 7. LCL growth maintenance assay using type 2 EBNA2 mutants.** (A) ER-EB 2.5
980 cells conditionally expressing an estrogen receptor type 1 EBNA2 fusion protein were cultured
981 in medium containing β-estradiol prior to resuspension in medium without β-estradiol. Cells
982 were transfected with OriP-based plasmids (p294) expressing full length type 1 or type 2
983 EBNA2 or the type 2 SD, motif 3 or SD and motif 3 mutant EBNA2 proteins and cultured in
984 medium without β-estradiol. Live cells (that excluded Trypan Blue) were counted 1, 2, 3 and
985 4 weeks post-transfection. Data from a representative experiment of 4 independent repeats is
986 shown. Error bars show the mean ± standard deviation of duplicate cell counts for each sample.
987 (B) Western blot analysis of EBNA2 expression in protein extracts from the transfected
988 EREB2.5 cells. Cells were harvested 2 days after transfection. EBNA2 was detected using the
989 PE2 monoclonal antibody and blots were probed for actin as a loading control.

990 **Figure 8. Western blot analysis of BS69 expression in EBV infected B cells.** (A) Western
991 blot analysis of BS69 expression in the EBV negative BL cell line AK31 and type 1 and type
992 2 EBV immortalised LCLs (that display the latency III pattern of gene expression associated
993 with expression of all EBV latent proteins). BS69 was detected using an antibody that
994 recognises a sequence in the MYND domain encoded by exon 15 (ab190890). EBNA2 was
995 detected using the PE2 monoclonal antibody. Type 2 EBV has a lower molecular weight due a
996 difference in the number of proline repeat residues present. Blots were probed for actin as a
997 loading control. (B) Western blot analysis of BS69 expression in EBV negative (BJAB, DG75,
998 AK31) and EBV positive latency I (Akata and Mutu I) and latency III B cell lines (Mutu III
999 (BL) and IB4 (LCL) as in A. (C) Western blot analysis of BS69 expression on primary B cell
1000 infection. UI indicates uninfected primary B cells. Samples were taken at the indicated day
1001 post-infection and analysed as in A.

1002

1003 **Figure 9. PCR analysis of the BS69 isoforms expressed in EBV infected B cells.** (A)
1004 Diagram of the four experimentally verified BS69 isoforms. The position of the start codon
1005 (ATG) and stop codon (red asterisk) is indicated. Numbering of exons is *as per* the canonical
1006 isoform (isoform 1). Exon lengths are not to scale. Exon 4 is shown in red, Exon 15 is shown
1007 in green and exon 14 is shown in blue. The 3' part of exon 14 present in isoforms 3 and 4 is
1008 shown in blue hatched lines. A sequence within exon 15 is recognised by the antibody
1009 (ab190890) used in Figure 8 as indicated on the diagram. Approximate locations of primers
1010 used for conventional PCR and QPCR are indicated by black and red arrows respectively. (B)
1011 Agarose gel analysis of PCR products generated using primers located in specific BS69 exons.
1012 The upper panel shows the PCR products amplified from cDNA samples from type 1 and type
1013 2 LCLs and the primary infection samples shown in C using a forward primer located in exon
1014 3 and a reverse primer located in exon 13. Transcripts containing exon 4 (isoform 1 and 3) will

1015 generate a 1139 bp product and those lacking exon 4 (isoforms 2 and 4) will produce a 977 bp
1016 product. The lower panel shows PCR carried out using the exon 3 forward primer and a reverse
1017 primer in the 3' region of exon 14 that is uniquely present in differentially spliced BS69
1018 transcripts lacking exon 15 (isoforms 3 and 4). Transcripts containing exon 4 and lacking exon
1019 15 (isoform 3) will generate a 1578 bp product and those lacking exon 4 and exon 15 will
1020 produce a 1416 bp product (isoform 4). (C) QPCR analysis of cDNA from a panel of EBV
1021 negative and positive B cell lines and primary EBV infections using primers that amplify across
1022 the exon 14 and exon 15 junction. For EBV infections, samples from two different experiments
1023 (#1 and #2) were used. Primary B cells (uninfected, UI) were infected with EBV and samples
1024 harvested after 2 days (+ EBV). Results show the mean ± standard deviation of QPCR
1025 replicates from a representative experiment. BS69 relative quantities were normalized to β2
1026 microglobulin. (D) QPCR analysis as in (C) using primers within exon 14. The reverse primer
1027 is located in the 3' part of exon 14 only present in BS69 isoform 3 and 4.

1028

1029 **Figure 10. Expression of a dominant negative form of BS69 increases EBNA2**
1030 **transactivation.** Transactivation assays in BJAB cells using EBNA2-GAL4-DNA binding
1031 domain fusion proteins and a GAL4 reporter plasmid. Cells were cotransfected with 300 ng of
1032 either type 1 GAL4-DBD:EBNA2 (aa 334-487) or type 2 GAL4-DBD:EBNA2 (301-454)
1033 constructs, 500 ng of pFRLuc (Gal4 firefly luciferase reporter), 10 ng of pRL-CMV and 1 μg
1034 of BS69 (pCI-BS69) or BS69 ΔMYND (pCI-BS69-ΔMYND) expressing plasmids. For each
1035 sample, firefly luciferase values were normalised for transfection efficiency using Renilla
1036 luciferase values. Results are presented as luciferase activity relative to the pFR-Luc reporter
1037 plasmid plus empty vector (pcDNA3.1-GAL4-DBD). BS69 ΔMYND was also transfected in
1038 the absence of EBNA2 expressing constructs. Results show the mean of two independent
1039 experiments ± standard deviation.

1040

1041 **Table 1.** Size exclusion chromatography and multiangle might scattering (MALS)
1042 determination of the molecular weight of individual type 1 and type 2 EBNA2 polypeptides,
1043 $BS69_{CC\text{-}MYND}$ and EBNA2-BS69 complexes. Theoretical and experimentally determined
1044 molecular weights are shown. For EBNA2-BS69 complexes, the theoretical molecular weights
1045 of complexes containing different numbers of EBNA2 and BS69 molecules are shown in
1046 parentheses. The most likely solution state based the experimentally determined molecular
1047 weight is indicated for each sample.

1048

1049 **Supporting Information Legends**

1050 **Supplementary Figure S1.** Normalised (dimensionless) Kratky plots generated using ScÅtter
1051 (v3.0 by Robert P. Rambo; Diamond Light Source). $I(q)/I(0)*(q*Rg)^2$ vs q*Rg. Scattering
1052 intensity I (q), scattering vector (q), radius of gyration (Rg).

1053

1054 **Supplementary Figure S2.** Solution structures of $BS69_{CC\text{-}MYND}$ and type 1 and type 2 EBNA2
1055 polypeptides determined by SAXS. (A-C) The SAXS envelopes (grey mesh) were generated
1056 by averaging 20 *ab-initio* models using the DAMMIF programme and further refined with
1057 DAMMIN to produce refined dummy atom models (magenta mesh). The maximum dimension
1058 (D_{max}) and volume were calculated using the ScÅtter programme. In (A) the $BS69_{CC\text{-}MYND}$
1059 dimer structure (cyan; PDB ID: 5HDA) was manually docked into the envelope. (D-F) SAXS
1060 scattering data (black dots) fitted to the *ab initio* DAMMIN dummy atom (red line). χ^2 values
1061 for fitting are shown.

1062

1063 **Supplementary Figure S3.** Alternative models and their respective goodness-of-fit to the
1064 experimental SAXS data. (A) One $BS69_{CC\text{-}MYND}$ dimer (cyan; PDB ID: 5HDA) and the *ab*
1065 *initio* model of one type 1 $EBNA2_{381\text{-}455}$ polypeptide (salmon) were manually docked into the
1066 *ab initio* envelope (grey mesh) of the type 1 EBNA2 BS69 complex. (B) SAXS scattering data
1067 were fitted to the docked structural complex shown in A and gave a χ^2 of 13.33 using FoXS.
1068 Graphs show relative log intensity vs scattering vector (q) (upper panel) and the deviation
1069 (residual) of the model from the experimental data (lower panel). The hydration parameter (C_2)
1070 was fixed to 0 to prevent the hydration shell increasing to beyond the maximum limit of 4 to
1071 attempt to fit the structure into the envelope. (C) The structural model shown in Figure 4C (two
1072 $BS69_{CC\text{-}MYND}$ dimers and two type 1 $EBNA2_{381\text{-}455}$ polypeptides) was refitted to the SAXS
1073 envelope using FoXS with the C_2 value set to 0 for comparison. This gave a similar χ^2 (2.59)
1074 to that shown in Figure 4A indicating a much better fit to the scattering data. (D) Two $BS69_{CC\text{-}}$
1075 $_{MYND}BS69_{CC\text{-}MYND}$ dimers (cyan; PDB ID: 5HDA) and the *ab initio* model of one type 2
1076 $EBNA2_{348\text{-}422}$ polypeptide (orange) were manually docked into the *ab initio* envelope (grey mesh). (E)
1077 SAXS scattering data were fitted to the docked structural complex shown in D and gave a χ^2 of 4.65
1078 using FoXS. Graphs show relative log intensity vs scattering vector (q) (upper panel) and the deviation
1079 (residual) of the model from the experimental data (lower panel). The hydration parameter (C_2) was
1080 fixed to 0 to prevent the hydration shell increasing to high levels to attempt to fit the structure into the
1081 envelope. (E) The structural model shown in Figure 4D (three $BS69_{CC\text{-}MYND}$ dimers and two type 2
1082 $EBNA2_{348\text{-}422}$ polypeptides) was refitted to the SAXS envelope using FoXS with the C_2 value set to 0
1083 for comparison. This gave a similar χ^2 (1.47) to that shown in Figure 4B indicating a much better fit to
1084 the scattering data.

1085

1086 **Supplementary Table S1**. Primer sequences.

1087

1088 **Supplementary Table S2.** Data obtained from Isothermal calorimetry analysis of EBNA2
1089 peptides and polypeptides binding to $BS69_{CC\text{-}MYND}$ (n.d. indicates binding not detected). Data
1090 show the mean ± standard deviation for three independent experiments. For peptides n values
1091 were fixed to 1. Data from type 2 EBNA2 peptides and polypeptides are in shaded columns.

1092

1093 **Supplementary Table S3.** SAXS data for BS69 and EBNA2 polypeptides and complexes.

1094

1095

1096

1097 **References**

1098 1. Cohen JI, Wang F, Mannick J, Kieff E. Epstein-Barr virus nuclear protein 2 is a key
1099 determinant of lymphocyte transformation. Proc Natl Acad Sci U S A. 1989
1100 Dec;86(23):9558-62. PubMed PMID: 2556717.
1101 2. Kempkes B, Ling PD. EBNA2 and Its Coactivator EBNA-LP. Curr Top Microbiol
1102 Immunol. 2015;391:35-59. PubMed PMID: 26428371.
1103 3. Glaser LV, Rieger S, Thumann S, Beer S, Kuklik-Roos C, Martin DE, et al. EBF1
1104 binds to EBNA2 and promotes the assembly of EBNA2 chromatin complexes in B cells.
1105 PLoS Pathog. 2017 Oct;13(10):e1006664. PubMed PMID: 28968461. Pubmed Central
1106 PMCID: 5638620.
1107 4. West MJ. Chromatin reorganisation in Epstein-Barr virus-infected cells and its role in
1108 cancer development. Current opinion in virology. 2017 Sep 11;26:149-55. PubMed PMID:
1109 28910751.
1110 5. Zhao B, Zou J, Wang H, Johannsen E, Peng CW, Quackenbush J, et al. Epstein-Barr
1111 virus exploits intrinsic B-lymphocyte transcription programs to achieve immortal cell growth.
1112 Proc Natl Acad Sci U S A. 2011 Sep 6;108(36):14902-7. PubMed PMID: 21746931. Pubmed
1113 Central PMCID: 3169132. Epub 2011/07/13. eng.
1114 6. Wood CD, Veenstra H, Khasnis S, Gunnell A, Webb HM, Shannon-Lowe C, et al.
1115 MYC activation and BCL2L11 silencing by a tumour virus through the large-scale
1116 reconfiguration of enhancer-promoter hubs. eLife. 2016 Aug 04;5. PubMed PMID:
1117 27490482. Pubmed Central PMCID: 5005034.
1118 7. Wang L, Grossman SR, Kieff E. Epstein-Barr virus nuclear protein 2 interacts with
1119 p300, CBP, and PCAF histone acetyltransferases in activation of the LMP1 promoter. Proc
1120 Natl Acad Sci U S A. 2000 Jan 4;97(1):430-5. PubMed PMID: 10618435.
1121 8. Wu DY, Kalpana GV, Goff SP, Schubach WH. Epstein-Barr virus nuclear protein 2
1122 (EBNA2) binds to a component of the human SNF-SWI complex, hSNF5/Ini1. J Virol. 1996
1123 Sep;70(9):6020-8. PubMed PMID: 8709224.
1124 9. Wu DY, Krumm A, Schubach WH. Promoter-specific targeting of human SWI-SNF
1125 complex by Epstein-Barr virus nuclear protein 2. J Virol. 2000 Oct;74(19):8893-903.
1126 PubMed PMID: 10982332.
1127 10. Tong X, Drapkin R, Reinberg D, Kieff E. The 62- and 80-kDa subunits of
1128 transcription factor IIH mediate the interaction with Epstein-Barr virus nuclear protein 2.
1129 Proc Natl Acad Sci U S A. 1995 Apr 11;92(8):3259-63. PubMed PMID: 7724549.
1130 11. Tong X, Drapkin R, Yalamanchili R, Mosialos G, Kieff E. The Epstein-Barr virus
1131 nuclear protein 2 acidic domain forms a complex with a novel cellular coactivator that can
1132 interact with TFIIE. Mol Cell Biol. 1995 Sep;15(9):4735-44. PubMed PMID: 7651391.
1133 12. Tong X, Wang F, Thut CJ, Kieff E. The Epstein-Barr virus nuclear protein 2 acidic
1134 domain can interact with TFIIB, TAF40, and RPA70 but not with TATA-binding protein. J
1135 Virol. 1995 Jan;69(1):585-8. PubMed PMID: 7983760.
1136 13. Cohen JI, Kieff E. An Epstein-Barr virus nuclear protein 2 domain essential for
1137 transformation is a direct transcriptional activator. J Virol. 1991 Nov;65(11):5880-5. PubMed
1138 PMID: 1656076.
1139 14. Sample J, Young L, Martin B, Chatman T, Kieff E, Rickinson A. Epstein-Barr virus
1140 types 1 and 2 differ in their EBNA-3A, EBNA-3B, and EBNA-3C genes. J Virol. 1990
1141 Sep;64(9):4084-92. PubMed PMID: 2166806.
1142 15. Dambaugh T, Hennessy K, Chamnankit L, Kieff E. U2 region of Epstein-Barr virus
1143 DNA may encode Epstein-Barr nuclear antigen 2. Proc Natl Acad Sci U S A. 1984
1144 Dec;81(23):7632-6. PubMed PMID: 6209719. Pubmed Central PMCID: 392202.

1145 16. Rowe M, Young LS, Cadwallader K, Petti L, Kieff E, Rickinson AB. Distinction
1146 between Epstein-Barr virus type A (EBNA 2A) and type B (EBNA 2B) isolates extends to
1147 the EBNA 3 family of nuclear proteins. J Virol. 1989 Mar;63(3):1031-9. PubMed PMID:
1148 2536817. Pubmed Central PMCID: 247795.
1149 17. Palser AL, Grayson NE, White RE, Corton C, Correia S, Ba Abdullah MM, et al.
1150 Genome diversity of Epstein-Barr virus from multiple tumor types and normal infection. J
1151 Virol. 2015 May;89(10):5222-37. PubMed PMID: 25787276. Pubmed Central PMCID:
1152 4442510.
1153 18. Correia S, Bridges R, Wegner F, Venturini C, Palser A, Middeldorp JM, et al.
1154 Sequence variation of Epstein-Barr virus: viral types, geography, codon usage and diseases. J
1155 Virol. 2018 Aug 15. PubMed PMID: 30111570.
1156 19. Rickinson AB, Young LS, Rowe M. Influence of the Epstein-Barr virus nuclear
1157 antigen EBNA 2 on the growth phenotype of virus-transformed B cells. J Virol. 1987
1158 May;61(5):1310-7. PubMed PMID: 3033261. Pubmed Central PMCID: 254104.
1159 20. Cancian L, Bosshard R, Lucchesi W, Karstegl CE, Farrell PJ. C-terminal region of
1160 EBNA-2 determines the superior transforming ability of type 1 Epstein-Barr virus by
1161 enhanced gene regulation of LMP-1 and CXCR7. PLoS Pathog. 2011 Jul;7(7):e1002164.
1162 PubMed PMID: 21857817. Pubmed Central PMCID: 3145799.
1163 21. Tzellos S, Correia PB, Karstegl CE, Cancian L, Cano-Flanagan J, McClellan MJ, et
1164 al. A Single Amino Acid in EBNA-2 Determines Superior B Lymphoblastoid Cell Line
1165 Growth Maintenance by Epstein-Barr Virus Type 1 EBNA-2. J Virol. 2014 Aug
1166 15;88(16):8743-53. PubMed PMID: 24850736.
1167 22. Lucchesi W, Brady G, Dittrich-Breiholz O, Kracht M, Russ R, Farrell PJ. Differential
1168 gene regulation by Epstein-Barr virus type 1 and type 2 EBNA2. J Virol. 2008
1169 Aug;82(15):7456-66. PubMed PMID: 18480445. Pubmed Central PMCID: 2493322. Epub
1170 2008/05/16. eng.
1171 23. Coleman CB, Daud, II, Ogolla SO, Ritchie JA, Smith NA, Sumba PO, et al. Epstein-
1172 Barr Virus Type 2 Infects T Cells in Healthy Kenyan Children. J Infect Dis. 2017 Sep
1173 15;216(6):670-7. PubMed PMID: 28934430. Pubmed Central PMCID: 5853903.
1174 24. Coleman CB, Wohlford EM, Smith NA, King CA, Ritchie JA, Baresel PC, et al.
1175 Epstein-Barr virus type 2 latently infects T cells, inducing an atypical activation characterized
1176 by expression of lymphotactic cytokines. J Virol. 2015 Feb;89(4):2301-12. PubMed PMID:
1177 25505080. Pubmed Central PMCID: 4338898.
1178 25. Coleman CB, Lang J, Sweet LA, Smith NA, Freed BM, Pan Z, et al. Epstein-Barr
1179 virus type-2 infects T-cells and induces B-cell lymphomagenesis in humanized mice. J Virol.
1180 2018 Aug 8. PubMed PMID: 30089703.
1181 26. Wen H, Li Y, Xi Y, Jiang S, Stratton S, Peng D, et al. ZMYND11 links histone
1182 H3.3K36me3 to transcription elongation and tumour suppression. Nature. 2014 Apr
1183 10;508(7495):263-8. PubMed PMID: 24590075. Pubmed Central PMCID: 4142212.
1184 27. Guo R, Zheng L, Park JW, Lv R, Chen H, Jiao F, et al. BS69/ZMYND11 reads and
1185 connects histone H3.3 lysine 36 trimethylation-decorated chromatin to regulated pre-mRNA
1186 processing. Mol Cell. 2014 Oct 23;56(2):298-310. PubMed PMID: 25263594. Pubmed
1187 Central PMCID: 4363072.
1188 28. de Rooij JD, van den Heuvel-Eibrink MM, Kollen WJ, Sonneveld E, Kaspers GJ,
1189 Beverloo HB, et al. Recurrent translocation t(10;17)(p15;q21) in minimally differentiated
1190 acute myeloid leukemia results in ZMYND11/MBTD1 fusion. Genes, chromosomes &
1191 cancer. 2016 Mar;55(3):237-41. PubMed PMID: 26608508.
1192 29. Wang J, Qin S, Li F, Li S, Zhang W, Peng J, et al. Crystal structure of human BS69
1193 Bromo-ZnF-PWWP reveals its role in H3K36me3 nucleosome binding. Cell Res. 2014
1194 Jul;24(7):890-3. PubMed PMID: 24675531. Pubmed Central PMCID: 4085756.

1195 30. Ladendorff NE, Wu S, Lipsick JS. BS69, an adenovirus E1A-associated protein,
1196 inhibits the transcriptional activity of c-Myb. Oncogene. 2001 Jan 4;20(1):125-32. PubMed
1197 PMID: 11244510.
1198 31. Masselink H, Vastenhouw N, Bernards R. B-myb rescues ras-induced premature
1199 senescence, which requires its transactivation domain. Cancer Lett. 2001 Sep 28;171(1):87-
1200 101. PubMed PMID: 11485831.
1201 32. Wei G, Schaffner AE, Baker KM, Mansky KC, Ostrowski MC. Ets-2 interacts with
1202 co-repressor BS69 to repress target gene expression. Anticancer research. 2003 May-
1203 Jun;23(3A):2173-8. PubMed PMID: 12894593.
1204 33. Velasco G, Grkovic S, Ansieau S. New insights into BS69 functions. J Biol Chem.
1205 2006 Jun 16;281(24):16546-50. PubMed PMID: 16565076.
1206 34. Ansieau S, Leutz A. The conserved Mynd domain of BS69 binds cellular and
1207 oncoviral proteins through a common PXLXP motif. J Biol Chem. 2002 Feb 15;277(7):4906-
1208 10. PubMed PMID: 11733528.
1209 35. Harter MR, Liu CD, Shen CL, Gonzalez-Hurtado E, Zhang ZM, Xu M, et al.
1210 BS69/ZMYND11 C-Terminal Domains Bind and Inhibit EBNA2. PLoS Pathog. 2016
1211 Feb;12(2):e1005414. PubMed PMID: 26845565. Pubmed Central PMCID: 4742278.
1212 36. Friberg A, Thumann S, Hennig J, Zou P, Nossner E, Ling PD, et al. The EBNA-2 N-
1213 Terminal Transactivation Domain Folds into a Dimeric Structure Required for Target Gene
1214 Activation. PLoS Pathog. 2015 May;11(5):e1004910. PubMed PMID: 26024477. Pubmed
1215 Central PMCID: 4449002.
1216 37. Kempkes B, Spitkovsky D, Jansen-Durr P, Ellwart JW, Kremmer E, Delecluse HJ, et
1217 al. B-cell proliferation and induction of early G1-regulating proteins by Epstein-Barr virus
1218 mutants conditional for EBNA2. Embo J. 1995 Jan 3;14(1):88-96. PubMed PMID: 7828599.
1219 38. Tsui S, Schubach WH. Epstein-Barr virus nuclear protein 2A forms oligomers in vitro
1220 and in vivo through a region required for B-cell transformation. J Virol. 1994 Jul;68(7):4287-
1221 94. PubMed PMID: 8207803. Pubmed Central PMCID: 236351.
1222 39. Harada S, Yalamanchili R, Kieff E. Epstein-Barr virus nuclear protein 2 has at least
1223 two N-terminal domains that mediate self-association. J Virol. 2001 Mar;75(5):2482-7.
1224 PubMed PMID: 11160754. Pubmed Central PMCID: 114834.
1225 40. Wan J, Zhang W, Wu L, Bai T, Zhang M, Lo KW, et al. BS69, a specific adaptor in
1226 the latent membrane protein 1-mediated c-Jun N-terminal kinase pathway. Mol Cell Biol.
1227 2006 Jan;26(2):448-56. PubMed PMID: 16382137. Pubmed Central PMCID: 1346911.
1228 41. Ikeda O, Sekine Y, Mizushima A, Oritani K, Yasui T, Fujimuro M, et al. BS69
1229 negatively regulates the canonical NF-kappaB activation induced by Epstein-Barr virus-
1230 derived LMP1. FEBS Lett. 2009 May 19;583(10):1567-74. PubMed PMID: 19379743.
1231 42. Ikeda O, Miyasaka Y, Yoshida R, Mizushima A, Oritani K, Sekine Y, et al. BS69
1232 cooperates with TRAF3 in the regulation of Epstein-Barr virus-derived LMP1/CTAR1-
1233 induced NF-kappaB activation. FEBS Lett. 2010 Mar 5;584(5):865-72. PubMed PMID:
1234 20138174.
1235 43. Ben-Bassat H, Goldblum N, Mitrani S, Goldblum T, Yoffey JM, Cohen MM, et al.
1236 Establishment in continuous culture of a new type of lymphocyte from a "Burkitt like"
1237 malignant lymphoma (line D.G.-75). Int J Cancer. 1977 Jan;19(1):27-33. PubMed PMID:
1238 188769. Epub 1977/01/01. eng.
1239 44. Jenkins PJ, Binne UK, Farrell PJ. Histone acetylation and reactivation of Epstein-Barr
1240 virus from latency. J Virol. 2000 Jan;74(2):710-20. PubMed PMID: 10623733. Pubmed
1241 Central PMCID: 111591. Epub 2000/01/07. eng.
1242 45. Klein G. Studies on Epstein-Barr Virus Genome and Ebv-Determined Nuclear
1243 Antigen in Human Malignant Disease. Cold Spring Harbor symposia on quantitative biology.
1244 1974;39:783-90. PubMed PMID: WOS:A1974AB46200012. English.

1245 46. Takada K. Cross-linking of cell surface immunoglobulins induces Epstein-Barr virus
1246 in Burkitt lymphoma lines. Int J Cancer. 1984 Jan 15;33(1):27-32. PubMed PMID: 6319296.
1247 47. Gregory CD, Rowe M, Rickinson AB. Different Epstein-Barr virus-B cell interactions
1248 in phenotypically distinct clones of a Burkitt's lymphoma cell line. J Gen Virol. 1990 Jul;71 (
1249 Pt 7):1481-95. PubMed PMID: 2165133. Epub 1990/07/01. eng.
1250 48. Spender LC, Lucchesi W, Bodelon G, Bilancio A, Karstegl CE, Asano T, et al. Cell
1251 target genes of Epstein-Barr virus transcription factor EBNA-2: induction of the p55alpha
1252 regulatory subunit of PI3-kinase and its role in survival of EREB2.5 cells. J Gen Virol. 2006
1253 Oct;87(Pt 10):2859-67. PubMed PMID: 16963743. Epub 2006/09/12. eng.
1254 49. Brocard M, Khasnis S, Wood CD, Shannon-Lowe C, West MJ. Pumilio directs
1255 deadenylation-associated translational repression of the cyclin-dependent kinase 1 activator
1256 RGC-32. Nucleic Acids Res. 2018 Jan 27. PubMed PMID: 29385536. Pubmed Central
1257 PMCID: 5909466.
1258 50. Franke D, Svergun DI. DAMMIF, a program for rapid ab-initio shape determination
1259 in small-angle scattering. J Appl Crystallogr. 2009 Apr;42:342-6. PubMed PMID:
1260 WOS:000264292800030. English.
1261 51. Volkov VV, Svergun DI. Uniqueness of ab initio shape determination in small-angle
1262 scattering. J Appl Crystallogr. 2003 Jun;36:860-4. PubMed PMID: WOS:000182284400105.
1263 English.
1264 52. Svergun DI. Restoring low resolution structure of biological macromolecules from
1265 solution scattering using simulated annealing (vol 76, pg 2879, 1999). Biophys J. 1999
1266 Nov;77(5):2896-. PubMed PMID: WOS:000083554900051. English.
1267 53. Schneidman-Duhovny D, Hammel M, Sali A. FoXS: a web server for rapid
1268 computation and fitting of SAXS profiles. Nucleic Acids Research. 2010 Jul;38:W540-W4.
1269 PubMed PMID: WOS:000284148900087. English.
1270 54. West MJ, Webb HM, Sinclair AJ, Woolfson DN. Biophysical and mutational analysis
1271 of the putative bZIP domain of Epstein-Barr virus EBNA 3C. J Virol. 2004 Sep;78(17):9431-
1272 45. PubMed PMID: 15308737.
1273 55. Bark-Jones SJ, Webb HM, West MJ. EBV EBNA 2 stimulates CDK9-dependent
1274 transcription and RNA polymerase II phosphorylation on serine 5. Oncogene. 2006 Mar
1275 16;25(12):1775-85. PubMed PMID: 16314842. Epub 2005/11/30. eng.
1276 56. McClellan MJ, Wood CD, Ojeniyi O, Cooper TJ, Kanhere A, Arvey A, et al.
1277 Modulation of enhancer looping and differential gene targeting by Epstein-Barr virus
1278 transcription factors directs cellular reprogramming. PLoS Pathog. 2013 Sep;9(9):e1003636.
1279 PubMed PMID: 24068937. Pubmed Central PMCID: 3771879. Epub 2013/09/27. eng.

1280

1281

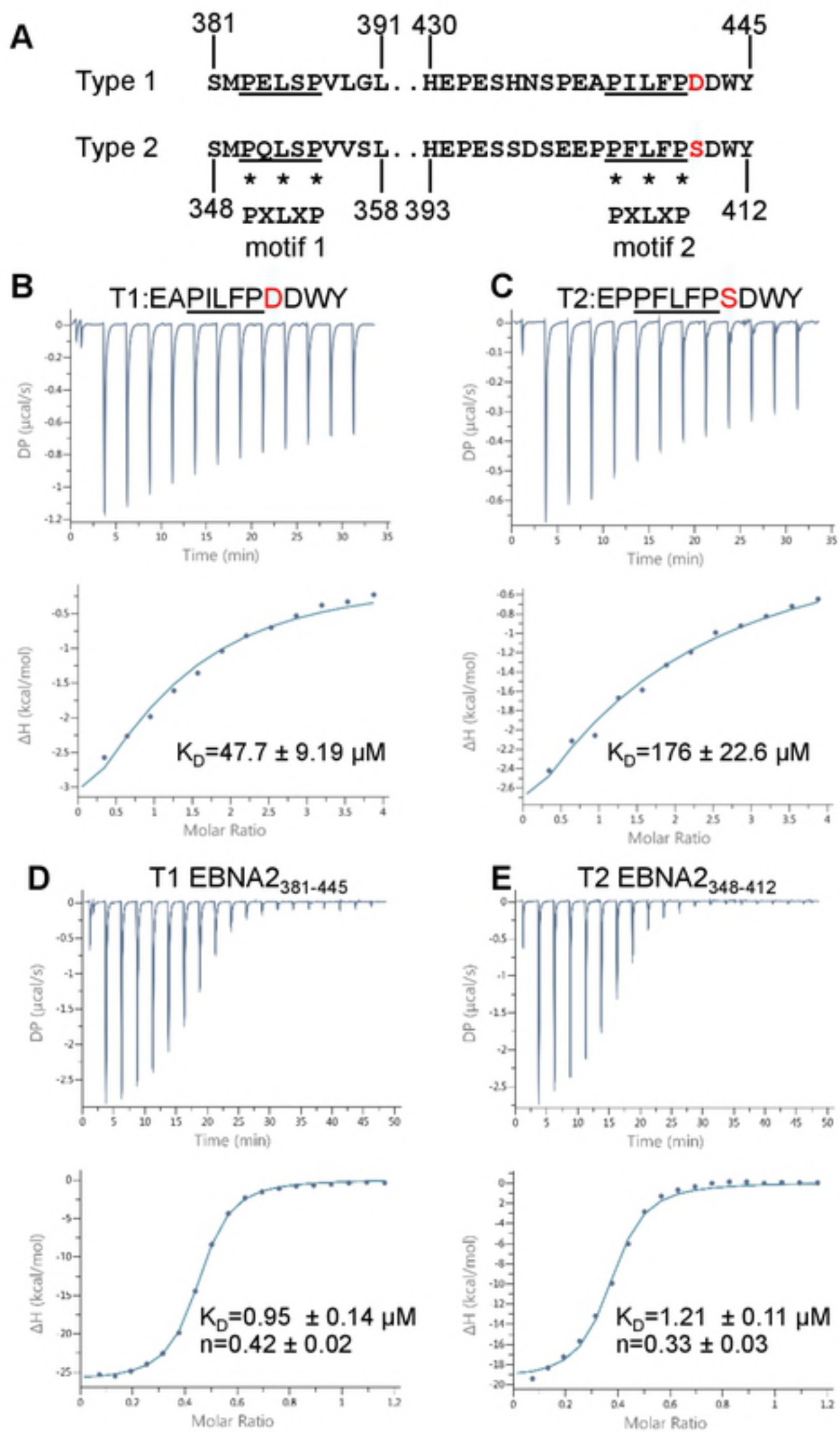

Figure 1

Main Figures combined file